European Journal of Medicinal Chemistry 279 (2024) 116845

Contents lists available at ScienceDirect

European Journal of Medicinal Chemistry

journal homepage: www.elsevier.com/locate/ejmech

Research paper

The multicomponent Passerini reaction as a means of accessing diversity in structure, activity and properties: Soft and hard vanilloid/cannabinoid modulators

Angela Lamberti [a,2], Marta Serafini [b,2,1], Silvio Aprile [b], Irene Preet Bhela [b], Georgia Goutsiou [b], Emanuela Pessolano [b], Gregorio Fernandez-Ballester [a], Antonio Ferrer-Montiel [a], Rita Maria Concetta Di Martino [b,*], Asia Fernandez-Carvajal [a,**], Tracey Pirali [b]

[a] Instituto de Investigación, Desarrollo e Innovación en Biotecnología Sanitaria de Elche (IDiBE), Universidad Miguel Hernández, Elche, Spain
[b] Department of Pharmaceutical Sciences, Università Degli Studi Del Piemonte Orientale, Largo Donegani 2, 28100, Novara, Italy

ARTICLE INFO

Keywords:
TRPV1 channel
CB receptors
Passerini multicomponent reaction
Soft drug
Dual targeting
Polipharmacology

ABSTRACT

A growing body of evidence points to the existence of a crosstalk between the endovanilloid (EV)- and the endocannabinoid (EC) systems, leading to the concept of a single system based on a shared set of endogenous ligands and regulation mechanisms. The EV/EC system encompasses the ion channel TRPV1, the G protein coupled receptors CB1 and CB2, their endogenous ligands and the enzymes for biosynthesis and inactivation. Disorders in which the EV/EC interaction is involved are inflammation, pain, neurodegenerative diseases and disorders of bones and skin.

In the present paper, with the aim of targeting the EV/EC system, the Passerini reaction is used in a diversity-oriented approach to generate a series of α-acyloxycarboxamides bearing different substructures that resemble endogenous ligands. Compounds have been screened for activity on TRPV1, CB1 and CB2 and metabolic stability in skin cells, liver subcellular fractions and plasma. This protocol allowed to generate agents characterized by a diverse activity on TRPV1, CB1 and CB2, as well as heterogeneous metabolic stability that could allow different routes of administration, from soft drugs for topical treatment of skin diseases to hard drugs for systemic use in inflammation and pain. Compared to natural mediators, these compounds have a better drug-likeness. Among them, **41** stands out as an agonist endowed with a well-balanced activity on both TRPV1 and CB2, high selectivity over TRPM8, TRPA1 and CB1, metabolic stability and synthetic accessibility.

1. Introduction

Transient receptor potential (TRP) channel superfamilies include multifunctional signalling proteins that, given their implication in cellular physiology and sensory perception, represent attractive targets for drug discovery and development efforts [1,2]. The most well-characterized and extensively studied TRP channel is the thermosensory channel TRP vanilloid 1 (TRPV1), also known as capsaicin receptor [3]. It is a ligand-gated non-selective cation channel highly expressed on primary neurons, where it acts as an integrator of painful stimuli, induced by pungent chemicals and high temperatures, and as an initiator of neurogenic inflammation [1]. TRPV1 is also expressed outside the sensory nervous system, in various brain nuclei and non-neuronal cells (*e.g.*, immune cells, adipocytes, skeletal and smooth muscle cells) [1], as well as in the peripheral terminals of nociceptors, keratinocytes and sebocytes. It therefore plays a pivotal role not only in temperature sensing, but also in the modulation of skin barrier function, in pain and pruritus [4]. Cryogenic-electron microscopy (Cryo-EM) and X-ray crystallography [5–7] have provided novel insights into TRPV1 structure and function and highlighted several druggable sites, driving the design of both novel agonists and antagonists [7,8].

Capsaicin is one the most clinically used TRPV1 agonists: topical

* Corresponding author.
** Corresponding author.
E-mail addresses: rita.dimartino@uniupo.it (R.M.C. Di Martino), asia.fernandez@umh.es (A. Fernandez-Carvajal).
[1] Present address: Department of Drug Science and Technology, Università di Torino, Via Pietro Giuria 9, 10125 Torino, Italy.
[2] These authors contributed equally to this work.

https://doi.org/10.1016/j.ejmech.2024.116845
Received 6 May 2024; Received in revised form 23 July 2024; Accepted 22 August 2024
Available online 7 September 2024

application of high concentration of capsaicin is effective in the management of peripheral pain due to desensitization of the channel. However, the initial TRPV1-coupled acute excitation and the associated burning sensation are a major clinical limitation that reduces patient's compliance and adherence to the treatment [9]. To avoid it, "non--pungent" TRPV1 agonists have been developed (*e.g.*, olvanil, Fig. 1 and MRD-652) [10], as well as various antagonists, some of which have been advanced into clinical trials [11,12]. Despite the huge potential of TRPV1 antagonists as painkillers, on-target adverse effects, namely hyperthermia and increased risk of burn injury due to compromised ability to detect painful stimuli, have so far hampered their clinical development. Topical administration has been therefore used to overcome this setback and to increase safety, while retaining efficacy in the treatment of skin disorders, as exemplified by asivatrep in atopic dermatitis (Fig. 1) [13] and resiniferatoxin (RTX) in osteoarthritic pain.

CB1 and CB2 belong to the cannabinoid receptor family of G protein coupled receptors (GPCRs) and are the biological targets of Δ^9-tetrahydrocannabinol (THC), the main psychoactive component in *Cannabis sativa* [14,15]. CB1 is highly expressed in central nervous system, mediates psychoactive effects, and modulates nociceptive pain [16], whereas CB2 is mainly located in immune cells with anti-inflammatory effects that indirectly contribute to anti-nociception of pain [17]. Of note, both these receptors are present in human skin, and in particular in keratinocytes, sensory neurons and immune cells, where they regulate epidermal homeostasis, pain sensation and skin inflammation [18]. The crystal and Cryo-EM structures of both CB1 and CB2 have been resolved and resolution of both binding pockets provided path for the rational drug design of novel ligands [19,20]. To avoid undesirable CB1-dependent side-effects associated with direct (*e.g.*, psychotropic effects, cognitive function impairment) or inverse (*e.g.*, anxiety and depression) agonists, efforts have been directed towards developing non-brain-penetrant modulators or CB2 selective agonists for treating pain and inflammatory states [14] and have led to the discovery of a set of chemical probes (*e.g.*, HU-910, HU-308 and JWH-133) [21]. However, when CB2 selective agonists entered clinical trials (*e.g.*, olorinab, GW-842,166X and S-777469, Fig. 1) [22], they did not result in successful drugs, mainly owing to insufficient efficacy [23].

A growing body of evidence has highlighted a cellular co-expression of CB and TRPV1: CB1 has been suggested to co-localize with TRPV1 in sensory and brain neurons [24], while CB2 co-localizes with the vanilloid channel in sensory neurons [25] and osteoclasts [26], pointing to a concerted action of the endovanilloid system (EVS) and the endocannabinoid one (ECS) in the modulation of biological responses. A functional crosstalk between the two systems has been found in neurons, where their interaction and bidirectional regulation shape excitability, even though this phenomenon is still being elucidated [27]. The topological and functional overlap between EVS and ECS has led to the definition of a merged "endovanilloid (EV)/endocannabinoid (EC) system", that includes CB1, CB2, TRPV1, their endogenous ligands and enzymes for biosynthesis and inactivation [28]. Disorders in which the EV/EC interaction is involved are inflammation [29], pain [30], bone disorders [26] and neurodegenerative diseases [31], along with multiple pathological conditions and disorders of skin [18,32,33].

Several modulators have been reported to act on both EVS and ECS, leading to an overlap between TRPV1 ligands and cannabinoids [34] to such an extent that TRPV1 channel has been named "ionotropic cannabinoid receptor" [33] and that some endocannabinoids are referred to as "endovanilloids" as they bind to TRPV1 as well (*e.g.*,

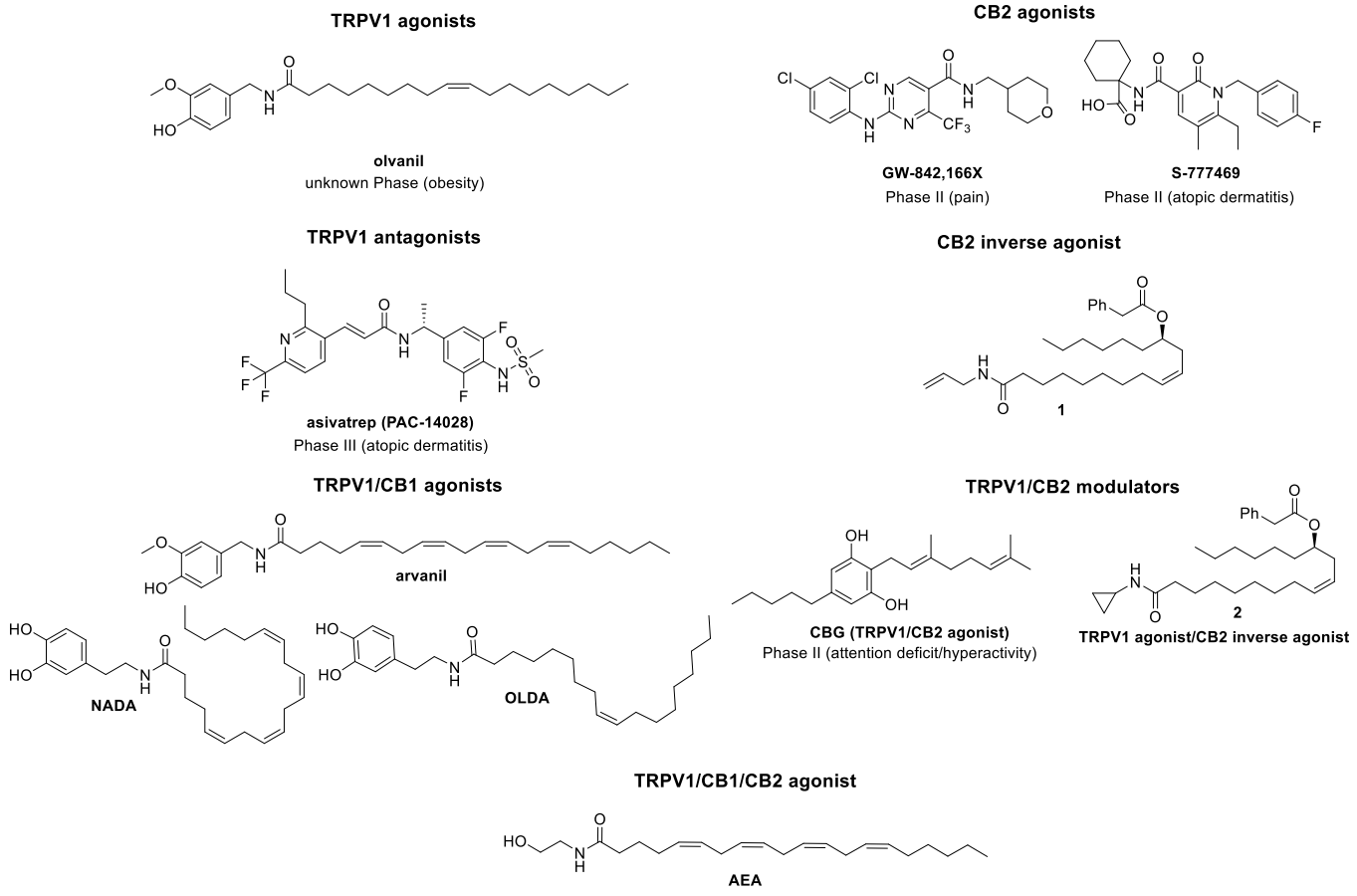

Fig. 1. Examples of vanilloid, cannabinoid and vanilloid/cannabinoid compounds. Only the therapeutic use corresponding to the most advanced clinical trial status is indicated according to the latest data from www.clinicaltrials.gov.

anandamide, AEA, Fig. 1 [35]; its dopamine-based analogues *N*-arachidonoyl-dopamine, NADA [36] and *N*-oleoyl-dopamine, OLDA, Fig. 1 [37]; and 2-arachidonoylglicerol, 2-AG [38]) [27]. Besides endocannabinoids, some synthetic cannabinoids (*e.g.*, ACPA-OH [39] and O-1811 [40]) and capsaicin-like derivatives (*e.g.*, arvanil, Fig. 1) [41] have been reported to directly modulate TRPV1 and CB1. With regard to TRPV1/CB2 modulation, both phytocannabinoids from *Cannabis* varieties (*e.g.*, cannabigerol, CBG, Fig. 1) [42] and synthetic cannabinoids (*e.g.*, HU-308, JWH-133 and WIN55,212-2) have been reported to activate both targets [21,43].

The observation that non-selective ligands produce stronger analgesic actions than those observed with pure agonists with the same affinity for each receptor type has sparked interest in the development of more rational, less serendipitous, and ameliorative multi-target approaches that address the EV/EC system at multiple levels [44]. Indeed, it is well-known that in the treatment of multi-factorial disorders the polipharmacological strategies might improve safety and efficacy properties with fewer side-effects compared to single-target molecules [45]. On this note, several multi-target drugs that modulate TRPV1 or cannabinoid receptors and enzymes have been reported as novel anti-inflammatory and analgesic agents [44,46–48]. With the advent of structural information, the identification of dual-acting chemotypes on both TRPV1 and CB1/CB2 might be assisted by computational approaches to rationalize the key structural features needed for activation of both TRPV1 and CB1 or CB2 [35,49].

By capitalizing on the advantages offered by multicomponent reactions (MCRs) in drug discovery [50], we followed up on our previous work, where we exploited the Passerini reaction [51] to access soft capsaicinoids bearing different substructures in correspondence of both the vanillyl head (Fig. 2, colored in pink) and the hydrophobic tail (Fig. 2, colored in light blue) [52–55]. The Passerini reaction is a MCR where an isocyanide, a carbonyl compound and a carboxylic acid react one-pot to afford an α-acyloxycarboxamide [56]. In 2018 our medicinal chemistry campaign resulted in the disclosure of a soft TRPV1 antagonist as a candidate for the topical treatment of pruritus devoid of hyperthermia (Fig. 2) [52]. According with the soft drug approach, an ester function was introduced as a soft spot in the vanilloid structure to circumscribe the action to the skin (Fig. 2, soft spot colored in orange): as soon as the compound exerts its activity, the soft spot undergoes hydrolysis, leading to inactive metabolites. Moreover, the halogen at position 6 (Fig. 2, iodide colored in green) caused a switch in activity from agonism to antagonism, as suggested by previous reports in the literature [57].

The main goal of the soft drug design is to control and direct metabolism toward the formation of inactive and/or non-toxic metabolites. For this reason, it relies on the incorporation of a soft spot, such as an ester function, to redirect oxidative metabolic biotransformation into inactivation *via* a hydrolytic pathway. The soft drug approach has gained interest for developing topical drugs with an improved safety profile, as these agents are highly stable in the target tissue and undergo rapid inactivation in the blood and/or liver [58]. In this respect, owing to the presence of a hydrolysable ester function, Passerini adducts α-acyloxycarboxamides represent an excellent source of soft-drugs. Interestingly, they have been reported to have variable stability according to the nature of substituents, spanning from highly hydrolytically labile compounds to exceptionally stable ones [59].

In this work, we leveraged the versatility of the Passerini reaction to access a library of compounds highly diverse in terms of structure, biological profile, and metabolic stability and capable of modulating the EV/EC system. We demonstrated that, by simply varying the nature of the building blocks in the MCR, it is possible to obtain a heterogenous library of hit compounds, including single- and dual-acting agents, endowed with high synthetic feasibility and finely tunable metabolic stability, spanning from soft drugs for topical treatment of skin diseases to hard drugs for systemic use in inflammation and pain.

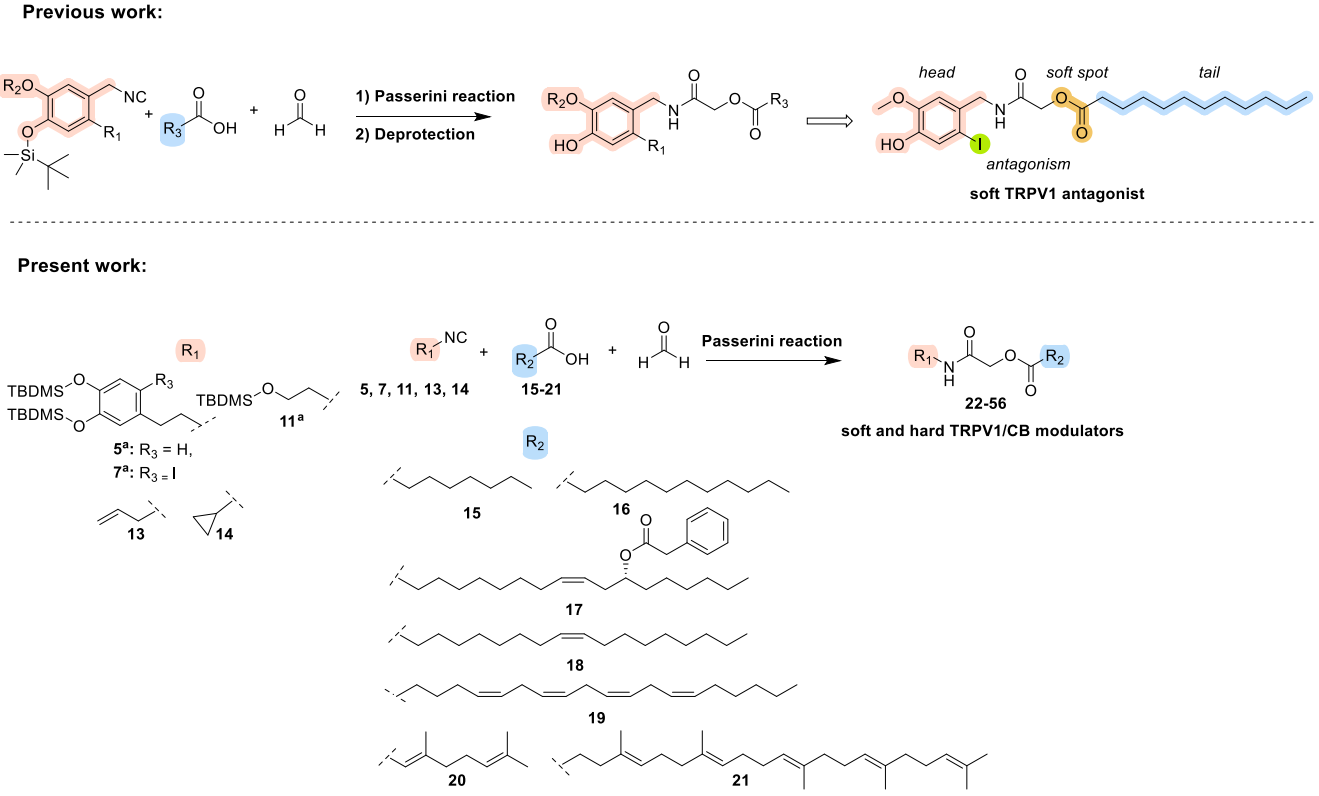

Fig. 2. The use of Passerini reaction to access TRPV1/CB modulators. [a]A final deprotection reaction was required to access the final compounds.

2. Results and discussion

2.1. Chemistry

To design our modulators we took inspiration from endocannabinoids known to act on TRPV1 channel (AEA, NADA and OLDA, Fig. 1) and from synthetic cannabinoids reported in the literature as CB2 inverse agonist (compound **1**, Fig. 1) and as dual TRPV1/CB ligands (compound **2**, Fig. 1) [43]. Among all the TRPV1/CB modulators reported to date, we focused on these five hits as they bear the amide substructure with the head on the secondary nitrogen and the tail at the alfa position and fit well to the synthesis of α-acyloxycarboxamide analogues by the Passerini reaction. Moreover, they show a diverse biological profile that might lead to a library of compounds endowed with a heterogenous activity. As an additional element of structural diversity, we also explored the introduction at the 6 position of the dopamine derivatives NADA and OLDA of an iodide to investigate whether this substitution confers antagonism on TRPV1 as already reported [52,59].

To perform the Passerini reaction, isocyanides bearing five different substructures (*i.e.*, 3,4-dihydroxyphenetyl-, **5**; 4,5-dihydroxy-2-iodophenethyl, **7**; 2-hydroxyethyl, **11**; allyl, **13**; cyclopropyl, **14**; Fig. 2) were coupled with commercially available fatty carboxylic acids, both saturated (*i.e.,* octanoic acid, **15**; dodecanoic acid, **16**; Fig. 2) and unsaturated (*i.e.,* (*R*,*Z*)-12-(2-phenylacetoxy)octadec-9-enoic acid, **17**; oleic acid, **18**; arachidonic acid, **19**; geranic acid, **20**; turbinaric acid, **21**; Fig. 2). Finally, formaldehyde was used as the carbonyl component in order to avoid any substitution at the α-position of the amide moiety, in agreement with modulators already reported in the literature.

We first proceeded with the preparation of dopamine-based isocyanides **5** and **7** following the route depicted in Scheme 1. The two hydroxyl groups of dopamine **3** were initially protected using *tert*-butyldimethylsilyl chloride (TBDMSCl) and a formylation reaction with a 1:1 mixture of methyl formate/methanol afforded derivative **4**. The resulting formamide was either directly dehydrated with phosphoryl chloride to give the isocyanide **5** needed for the agonists or underwent a selective iodination to yield **6**, which reacted in a dehydration reaction to afford isocyanide **7** required for the synthesis of putative antagonists.

Reagents and conditions: (a) Imidazole, TBDMSCl, dry CH_2Cl_2, rt, overnight, 59 %; (b) HCOOMe/MeOH 1:1, K_2CO_3, 35 °C, 2h, 87 %; (c) $POCl_3$, TEA, dry CH_2Cl_2, 0 °C, 1h, 77–82 %; (d) I_2, CF_3COOAg, $CHCl_3$, rt, 45 min, 86 %.

tert-Butyl(2-isocyanoethoxy)dimethylsilane **11** was prepared *via* a three-step procedure shown in Scheme 2. First, a selective and quantitative protection of the hydroxyl group using TBDMSCl afforded 2-(TBDMS-oxy)ethanolamine (**9**), which underwent a formylation of the primary amine to give intermediate **10**. A final dehydration of the latter afforded the desired isocyanide **11**.

Reagents and conditions: (a) Imidazole, TBDMSCl, dry CH_2Cl_2, rt, 2h, 98 %; (b) HCOONa, CH_3COCl, rt, overnight, 73 %; (c) $POCl_3$, TEA, dry CH_2Cl_2, 0 °C, 1h, 99 %.

Lastly, a Hofmann isonitrile synthesis allowed to obtain allyl isocyanide **13** using the lipophilic phase-transfer catalyst benzyltriethylammonium chloride (TEBA) [60]. Due to its chemical instability, **13** was used as crude material in the following multicomponent step.

The Passerini reaction between the isocyanide (**5**, **7**, **11**, **13** and the commercially available cyclopropyl isocyanide **14**), the carboxylic acid (**15**–**21**) and formaldehyde was carried out as outlined in Scheme 3, affording the corresponding α-acyloxycarboxamides **22**–**56** with yields ranging from 18 to 82 % (Tables 1 and 2). To prepare compounds **22**–**42**, a final cleavage of the TBDMS group with tetra-*n*-butylammonium fluoride (TBAF) in the presence of acetic acid to prevent ester hydrolysis was used.

As the compounds were initially designed as soft drugs, metabolites of hydrolysis were prepared and assessed for their activity on the three targets. Indeed, prompt metabolism into inactive metabolites is a prerequisite when developing soft drugs. To this aim, 2-hydroxy-*N*-alkylacetamides have been prepared starting from the corresponding isocyanides (**5**, **7**, **11**, **13**, and **14**) according to a procedure previously reported [61] (Scheme 4). For the TBDMS-protected isocyanides **5** and **7**, a final deprotection reaction in the presence of TBAF gave the title metabolites **57**–**61**.

Reagents and conditions: (a) CH_2Cl_2, 40 °C, overnight, 67–96 % for compounds **60** and **61**; (b) CH_3COOH, TBAF, THF, 0 °C, 3h, 39–70 % (over two steps for compounds **57**–**59**).

2.2. Screening of the activity of the synthesized compounds by microfluorometric assays

The first series of compounds (Table 1) is composed of NADA and OLDA analogues bearing dopamine as polar head and characterized by a hydrogen (**22**–**28**) or iodine (**29**–**35**) at position 6 of the 3,4-dihydroxyphenethyl group or 2-position of the 4,5- dihydroxyphenethyl moiety. While the former have been designed as putative TRPV1 agonists, the latter are supposed to act as antagonists of the same channel given the presence of the halogen [52,59]. The activity of the compounds over TRPV1 ion channel and CB receptors was challenged by fluorometric assays using HEK293 cells stably expressing the human isoforms. The compounds were initially tested at four different concentrations (1, 10, 100 and 200 μM) and the potency of the compounds that were found to be active was calculated using 7 different concentrations from 0.01 to

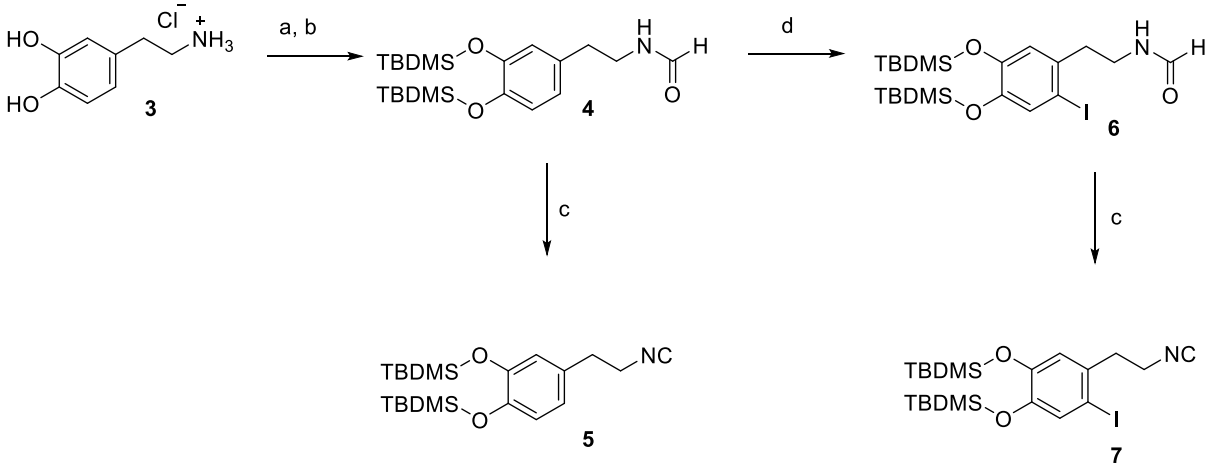

Scheme 1. Synthesis of NADA and OLDA isocyanides **5** and **7**.

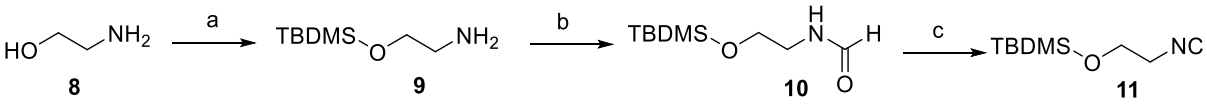

Scheme 2. Synthesis of the TBDMS-protected ethan-1-ol isocyanide 11.

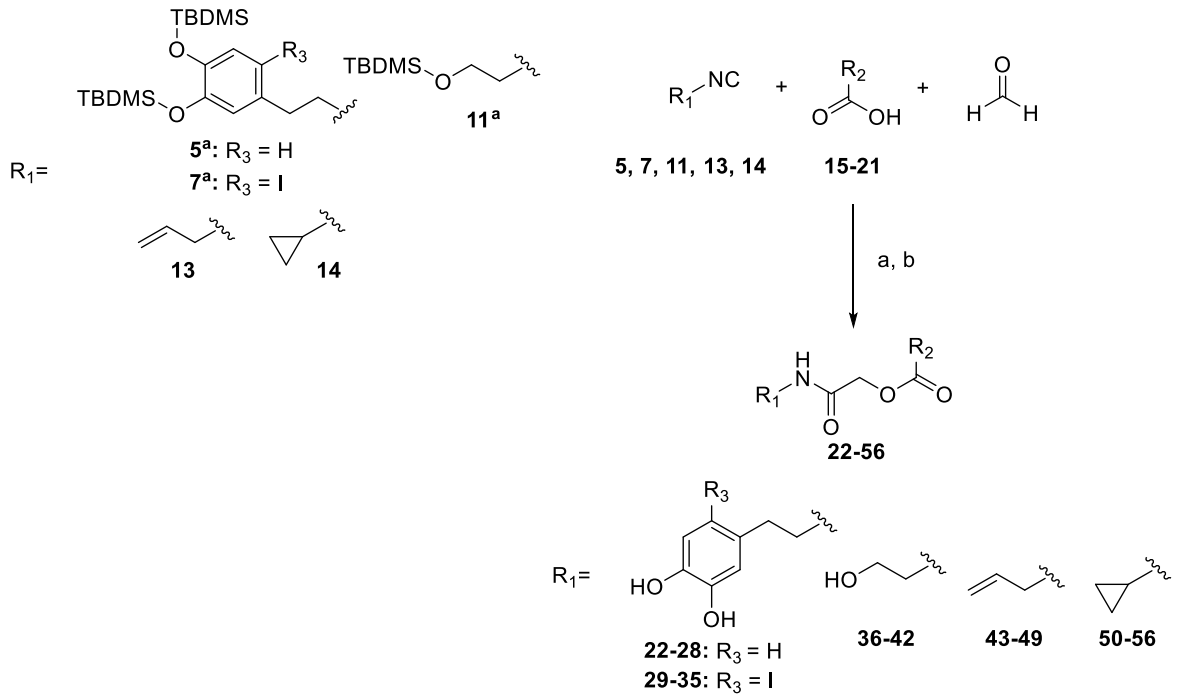

Scheme 3. General synthetic approach *via* Passerini reaction and deprotection.
Reagents and conditions: (a) CH2Cl2, 40 oC, rt, 2-4h, 18-91 %; a Compounds 22-42 underwent to a further deprotection reaction in line with the following conditions (b) CH3COOH, TBAF, THF, 0 oC, 2-3h, 18-82 %.

200 μM.

As expected, the first compounds **22**–**28** behave as TRPV1 agonists with EC_{50} values ranging from 0.3 to 10.6 μM. They are selective over CB receptors, except for **22** that also shows agonism at CB1 in the low micromolar range (EC_{50} = 13.9 μM) and **27** that displays CB1 and CB2 agonistic activity in the mid-micromolar range. Concerning agonism of **27** at CB receptors, experiments in control cells that did not express CB receptors highlighted an unspecific effect, putatively related to an inhibitory activity of adenylate cyclase (IC_{50} = 44.4 ± 1.9 μM).

Among the iodine-bearing compounds **29**–**35**, three derivatives (**29**, **30**, **34**) were shown to antagonize TRPV1 with IC_{50} values lower than 100 μM (IC_{50} = 54.2, 64.6, 9.8 μM, respectively), being **30** the only one selective over CB receptors. We could demonstrate that the insertion of the halogen on the dopamine scaffold might lead to antagonism on TRPV1 as for capsaicin and resiniferatoxin. Although **34** is the most potent TRPV1 antagonist, it showed agonist activity at both CB receptors in the mid-micromolar range and, similarly to **27**, it putatively inhibits adenylate cyclase with an IC_{50} value of 40.5 μM. Compound **29** also displayed agonism on CB2 receptor, albeit with an EC_{50} value exceeding 100 μM. The remaining compounds in this series showed no activity on the receptors when tested up to 200 μM.

The second series of compounds bear in correspondence of the head ethan-1-ol, allyl or cyclopropyl moiety (Table 2), resembling AEA (**36**–**42**), compound **1** (**43**–**49**) and compound **2** (**50**–**56**) respectively, and in correspondence of the tail the same fatty carboxylic acids as in the first series. All ethanolamine-based derivatives act as agonists of TRPV1 with EC_{50} values ranging from 0.4 to 26.8 μM. The closest analogue to AEA (**40**) shows a dual activity, albeit not well-balanced, on TRPV1 (EC_{50} = 2.1 μM) and CB1 (EC_{50} = 30.6 μM). On the other hand, the insertion of a shorter unsaturated tail led to **41**, which behaves as a TRPV1 (EC_{50} = 26.8 μM) and CB2 agonist (EC_{50} = 37.8 μM) with a good balance of the two activities. Compounds bearing the allylamine substructure share similar activities in terms of agonism on TRPV1 (EC_{50} = 2.4–36.4 μM) and show selectivity over CB receptors, except for **45** that behaves as an inverse agonist of CB2 and **47** that shows micromolar potency as agonist on both CB1 (EC_{50} = 16.6 μM) and CB2 (EC_{50} = 62.0 μM), although with a preference for the CB1 receptor. Finally, the cyclopropylamine-based derivatives are agonists of TRPV1, showing EC_{50} values from submicromolar to mid-micromolar range (EC_{50} = 0.7–33.1 μM). Concerning CB activity, the dodecanoate compound (**51**) shows agonism at CB2 (EC_{50} = 87.6 μM), while the (2-phenylacetoxy) octadec-9-enoate derivative (**52**) acts as a CB2 inverse agonist, with a higher potency than **45**. Furthermore, compounds **53** and **54** display micromolar agonism at CB1 (EC_{50} = 27.9 and 13.8 μM, respectively), and **56** shows less potency at the same receptor (EC_{50} = 195.5 μM).

The five metabolites were also evaluated for their activity on TRPV1, CB1 and CB2 at a concentration of 1 μM. No activity on cannabinoid receptors and very low activity on the TRPV1 channel were observed, with EC_{50} or IC_{50} values higher than 100 μM (Table 3).

2.3. Metabolic stability

Compounds **29**, **34**, **40**, **41**, **51**, **54** were selected as top-six TRPV1/CB modulators taking into consideration potency and selectivity or, alternatively, a dual targeting activity with a good balance on TRPV1 and CB1 or CB2, and were further characterized in terms of metabolic

Table 1
NADA and OLDA analogues.

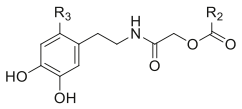

Cpd, Yield	R_3	R_2	hTRPV1		hCB1		hCB2	
			% Activity at 1 μM	**EC_{50}/IC_{50} (μM)**	**% Activity at 1 μM**	**EC_{50}/IC_{50} (μM)**	**% Activity at 1 μM**	**EC_{50}/IC_{50} (μM)**
Capsaicin				EC_{50} = 1 ± 0.02				
ruthenium red				IC_{50} = 0.51 ± 0.03				
CP-55,940						EC_{50} = 0.05 ± 0.001		EC_{50} = 0.02 ± 0.001
rimonabant						IC_{50} = 0.01 ± 0.0005		
AM630								IC_{50} = 0.03 ± 0.0007
22, 50 %	H	heptyl	23.5 ± 8.3	EC_{50} = 10.6 ± 2.2	8.2 ± 5.3	EC_{50} = 13.9 ± 1.6	n.a.	
23, 82 %	H	undecyl	17.2 ± 4.3	EC_{50} = 5.2 ± 1.0	n.a.		n.a.	
24, 44 %	H	(*R,Z*)-11-(2-phenylacetoxy)heptadec-8-en-1-yl	29.0 ± 7.6	EC_{50} = 3.1 ± 1.0	n.a.		n.a.	
25, 67 %	H	(*Z*)-heptadec-8-enyl	74.0 ± 5.6	EC_{50} = 0.5 ± 0.1	n.a.		n.a.	
26, 65 %	H	(4*Z*,7*Z*,10*Z*,13*Z*)-nonadeca-4,7,10,13-tetraen-1-yl	61.7 ± 8.8	EC_{50} = 1.0 ± 0.3	n.a.		n.a.	
27[a], 53 %	H	(*E*)-2,6-dimethylhepta-1,5-dien-1-yl	62.6 ± 9.2	EC_{50} = 0.7 ± 0.5	n.a.	EC_{50} = 118.0 ± 2.1	n.a.	EC_{50} = 89.9 ± 3.5
28, 18 %	H	(3*E*,7*E*,11*E*,15*E*)-3,7,12,16,20-pentamethylhenicosa-3,7,11,15,19-pentaen-1-yl	66.1 ± 3.6	EC_{50} = 0.3 ± 0.1	n.a.		n.a.	
29, 67 %	I	heptyl	12.7 ± 4.2	IC_{50} = 54.2 ± 2.5	n.a.		1.3 ± 0.5	EC_{50} > 100
30, 70 %	I	undecyl	15.0 ± 1.9	IC_{50} = 64.9 ± 2.6	n.a.		n.a.	
31, 39 %	I	(*R,Z*)-11-(2-phenylacetoxy)heptadec-8-en-1-yl	3.8 ± 1.5	IC_{50} > 100	n.a.		n.a.	
32, 61 %	I	(*Z*)-heptadec-8-enyl	2.7 ± 3.1	IC_{50} > 100	n.a.		n.a.	
33, 76 %	I	(4*Z*,7*Z*,10*Z*,13*Z*)-nonadeca-4,7,10,13-tetraen-1-yl	3.5 ± 1.6	IC_{50} > 100	n.a.		n.a.	
34[a], 43 %	I	(*E*)-2,6-dimethylhepta-1,5-dien-1-yl	28.7 ± 5.7	IC_{50} = 9.8 ± 0.8	n.a.	EC_{50} = 41.4 ± 1.6	n.a.	EC_{50} = 36.8 ± 1.6
35, 33 %	I	(3*E*,7*E*,11*E*,15*E*)-3,7,12,16,20-pentamethylhenicosa-3,7,11,15,19-pentaen-1-yl	8.2 ± 1.5	IC_{50} > 100	n.a.		n.a.	

n.a. = no activity was detected at concentrations above 200 μM.
Controls for TRPV1 agonism capsaicin and antagonism ruthenium red.
Controls for CB1 agonism CP-55,940 and antagonism rimonabant.
Controls for CB2 agonism CP-55,940 and antagonism AM630.
All determinations were performed in triplicate (n = 3) in 3 independent experiments (N = 3). All data are expressed as the mean ± standard deviation (SD).
[a] Unspecific effect on CB1/CB2: putative inhibition of adenylate cyclase IC_{50} = 44.4 ± 1.9 μM and 40.5 ± 1.5 μM for **27** and **34** respectively.

stability in the plasma, hepatic and cutaneous settings with the aim at discriminating between hard drugs (stable in the three compartments) and soft drugs (unstable in plasma and in the liver) (Table 4).

Compounds were first assessed in human plasma and liver S9 fraction by monitoring the residual substrate and the formation of the 2-hydroxy-*N*-alkylacetamide metabolite generated by ester enzymatic hydrolysis (Table 3 and Supporting Information, SI). Besides, the cutaneous metabolic stability was evaluated for the selected compounds in human skin S9 fraction and homogenates from immortalized keratinocytes (HaCaT), primary keratinocytes and fibroblasts (Table 4 and SI).

The performed experiments revealed that **41** is the only compound stable under all tested conditions thanks to the presence of the (*E*)-3,7-dimethylocta-2,6-dienoate side chain. Even though alkanoates containing ramification and unsaturation usually prevent compounds from enzymatic hydrolysis, compound **34** and, to a lesser extent, **40** and **54** are unstable in liver S9 fraction, while showing high stability in the other settings. Consistently with the known hydrolytic instability of esters bearing linear alkanoates, **29** and, to a lesser extent, **51** resulted the most unstable compounds of the series both in liver and skin S9. A low stability was observed also when the two compounds were incubated in fibroblast homogenates, while compound **51** showed higher stability than **29** in both HaCaT and keratinocyte homogenates.

Overall, susceptibility to enzymatic hydrolysis spanned from compound **29**, which showed high skin instability inappropriate even for soft drug purposes, to **34**, that behaves as a soft drug ideal for topical administration, to **41**, acting as a hard drug for systemic use.

Given its well-balanced activity on TRPV1 and CB2, the absence of activity on CB1 that might give rise to unwanted psychoactive effects, the exquisitely high chemical and metabolic stability in all the assessed systems, its potential in the treatment of inflammation and pain, **41** was selected for further characterization.

2.4. Characterization of compound 41

To provide direct evidence for activity on TRPV1, derivative **41** was tested in single HEK293 cells stably expressing the human TRPV1

Table 2
AEA, compounds **1** and **2** analogues.

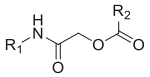

Cpd, Yield	R_1	R_2	hTRPV1		hCB1		hCB2	
			% Activity at 1 μM	**EC_{50} (μM)**	**% Activity at 1 μM**	**EC_{50} (μM)**	**% Activity at 1 μM**	**EC_{50} (μM)**
36, 40 %		Heptyl	15.8 ± 8.8	13.5 ± 1.1	n.a.		n.a.	
37, 49 %		Undecyl	10.2 ± 3.3	7.4 ± 1.2	n.a.		n.a.	
38, 20 %		(*R*,*Z*)-11-(2-phenylacetoxy)heptadec-8-en-1-yl	21.0 ± 6.3	3.7 ± 1.1	n.a.		n.a.	
39, 35 %		(*Z*)-heptadec-8-enyl	24.1 ± 9.7	1.9 ± 0.5	n.a.		n.a.	
40, 36 %		(4*Z*,7*Z*,10*Z*,13*Z*)-nonadeca-4,7,10,13-tetraen-1-yl	38.2 ± 7.2	2.1 ± 0.7	5.2 ± 2.6	30.6 ± 1.3	n.a.	
41, 42 %		(*E*)-2,6-dimethylhepta-1,5-dien-1-yl	13.2 ± 3.7	26.8 ± 2.4	n.a.		3.7 ± 1.1	37.8 ± 3.6
42, 44 %		(3*E*,7*E*,11*E*,15*E*)-3,7,12,16,20-pentamethylhenicosa-3,7,11,15,19-pentaen-1-yl	56.5 ± 7.2	0.4 ± 0.1	n.a.		n.a.	
43, 54 %		heptyl	14.4 ± 5.2	23.3 ± 3.7	n.a.		n.a.	
44, 50 %		undecyl	16.5 ± 6.4	11.4 ± 1.5	n.a.		n.a.	
45, 18 %		(*R*,*Z*)-11-(2-phenylacetoxy)heptadec-8-en-1-yl	16.3 ± 3.4	15.2 ± 1.5	n.a.		n.a.	inverse agonist[a]
46, 49 %		(*Z*)-heptadec-8-enyl	28.6 ± 8.3	4.7 ± 1.5	n.a.		n.a.	
47, 46 %		(4*Z*,7*Z*,10*Z*,13*Z*)-nonadeca-4,7,10,13-tetraen-1-yl	18.8 ± 2.5	21.8 ± 5.0	33.6 ± 5.3	16.6 ± 1.3	4.2 ± 2.1	62.0 ± 1.2
48, 50 %		(*E*)-2,6-dimethylhepta-1,5-dien-1-yl	42.8 ± 9.6	2.4 ± 0.7	n.a.		n.a.	
49, 43 %		(3*E*,7*E*,11*E*,15*E*)-3,7,12,16,20-pentamethylhenicosa-3,7,11,15,19-pentaen-1-yl	7.7 ± 3.6	36.4 ± 1.5	n.a.		n.a.	
50, 91 %		heptyl	24.9 ± 7.1	10.0 ± 5.0	n.a.		n.a.	
51, 79 %		undecyl	38.4 ± 6.6	1.7 ± 0.4	n.a.		2.4 ± 1.1	87.6 ± 4.0
52, 86 %		(*R*,*Z*)-11-(2-phenylacetoxy)heptadec-8-en-1-yl	42.5 ± 11.1	2.6 ± 0.9	n.a.		n.a.	inverse agonist[a]
53, 88 %		(*Z*)-heptadec-8-enyl	39.6 ± 3.7	0.7 ± 0.2	22.1 ± 4.2	27.9 ± 1.1	n.a.	
54, 90 %		(4*Z*,7*Z*,10*Z*,13*Z*)-nonadeca-4,7,10,13-tetraen-1-yl	8.9 ± 3.5	20.3 ± 1.7	28.8 ± 5.1	13.8 ± 1.5	n.a.	
55, 66 %		(*E*)-2,6-dimethylhepta-1,5-dien-1-yl	21.3 ± 1.3	33.1 ± 2.3	n.a.		n.a.	
56, 75 %		(3*E*,7*E*,11*E*,15*E*)-3,7,12,16,20-pentamethylhenicosa-3,7,11,15,19-pentaen-1-yl	19.9 ± 4.9	13.4 ± 4.3	2.1 ± 1.1	195.5 ± 2.0	n.a.	

All determinations were performed in triplicate (n = 3) in 3 independent experiments (N = 3). All data are expressed as the mean ± standard deviation (SD).
[a] The inverse agonism was assessed in the range of 25–200 μM.

isoform by patch-clamp recordings using a 100 ms voltage ramp ranging from −120 mV to +120 mV in 100 ms steps of 20 mV from a holding potential of 0 mV.

Before moving forward with patch-clamp recordings, we evaluated the solubility of **41** up to 100 μM concentration in the corresponding buffer (see Experimental Section), observing complete dissolution. Perfusion with 0.5 μM capsaicin activated a large, strongly outwardly rectifying current reversing at a potential around 10 mV (10.3 ± 4.1 mV; n = 6) (Fig. 3A, black trace). No currents were activated when capsaicin was perfused in non-transfected cells (Fig. 3A, orange trace). The

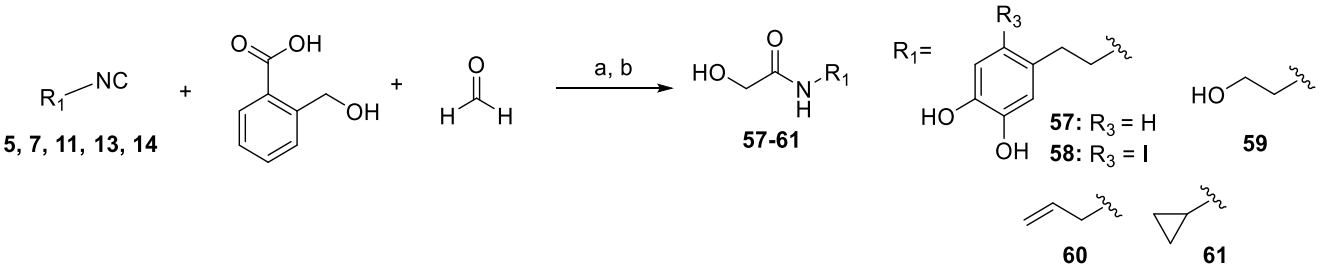

Scheme 4. Synthesis of metabolites **57-61**.

Table 3
Metabolites **59–61**.

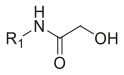

Cpd, Yield	R_1	hTRPV1		hCB1		hCB2	
		% Activity at 1 μM	EC_{50}/IC_{50} (μM)	% Activity at 1 μM	EC_{50} (μM)	% Activity at 1 μM	EC_{50} (μM)
57, 39 %	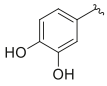	6.6 ± 6.2	EC_{50} > 100	n.a.	>100	n.a.	>100
58, 70 %	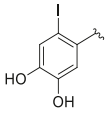	10.1 ± 2.3	IC_{50} > 100	n.a.	>100	n.a.	>100
59, 62 %		10.5 ± 4.0	EC_{50} > 100	n.a.	>100	n.a.	>100
60, 67 %		12.2 ± 3.7	EC_{50} > 100	n.a.	>100	n.a.	>100
61, 96 %		15.1 ± 4.9	EC_{50} > 100	n.a.	>100	n.a.	>100

All determinations were performed in triplicate (n = 3) in 3 independent experiments (N = 3). All data are expressed as the mean ± standard deviation (SD).

Table 4
Metabolic stability data for the selected compounds.

Cpd	Plasma 60 min	Liver S9 60 min	Skin S9 60 min	HaCaT 120 min	Kerat. 120 min	Fibrob. 120 min
29	13 % (± 0.78)	1 % (± 0.33)	27 % (± 0.48)	73 % (± 2.78)	85 % (± 0.98)	69 % (± 0.05)
34	>99 % (± 0.91)	2 % (± 0.36)	>99 % (± 2.83)	82 % (± 5.99)	87 % (± 12.6)	97 % (± 6.00)
40	>99 % (± 2.69)	24 % (± 1.34)	76 % (± 1.75)	>99 % (± 0.91)	97 % (± 0.89)	73 % (± 1.17)
41	89 % (± 1.25)	89 % (± 0.29)	96 % (± 1.58)	98 % (± 3.75)	96 % (± 0.53)	93 % (± 2.25)
51	80 % (± 0.76)	1 % (± 0.05)	69 % (± 0.80)	94 % (± 5.34)	99 % (± 4.27)	62 % (± 2.72)
54	76 % (± 0.62)	17 % (± 0.39)	80 % (± 0.72)	>99 % (± 3.39)	>99 % (± 0.52)	67 % (± 11.95)

*Metabolic stability data are expressed as remaining substrate percentage (± *standard error*) after incubation. Each experiment was performed in triplicate.

presence of capsazepine, a TRPV1 channel antagonist, produces blockade of the currents induced by both capsaicin (Fig. 3A, gray curve) and **41** (Fig. 3A, light green curve), indicating the specific effect of compound **41** on the channel. The dose-response curve for capsaicin-evoked currents at −60 mV showed an EC_{50} value of 0.3 ± 0.5 μM (Fig. 3B, black curve). Perfusion with 100 μM **41** also activated a large, strongly outwardly rectifying current reversing at a potential near 0 mV (3.5 ± 3.8 mV; n = 6) (Fig. 3A, blue trace). When compared to capsaicin, derivative **41** (Fig. 3B, blue curve) displayed lower potency (EC_{50} = 47.5 ± 1.0 μM *vs* 0.2 ± 0.2 μM; n = 7) and a similar efficacy (current density at +80 mV was 333 ± 145 pA/pF and 198 ± 44 pA/pF for capsaicin and **41**, respectively; p > 0.05) (Fig. 3A).

To evaluate the therapeutic potential of **41**, we tested its ability to induce TRPV1 desensitization on recombinantly expressed hTRPV1. As depicted in Fig. 4A, repeated application of capsaicin desensitized hTRPV1 channels, as evidenced by the lower percentage of current activated by the second (P2) capsaicin pulse (Fig. 4C, P2/P1 = 0.41 ± 0.1, n = 6). In the lower trace (Fig. 4B) the two consecutive pulses of **41**, interspersed by a washing period, produced the same TRPV1 desensitization (Fig. 4C, P2/P1 = 0.37 ± 0.05, n = 6). Furthermore, it can be observed that the longer exposure of the channel to **41** in the first pulse induced a fast TRPV1 inactivation that partially recovered after washing the compound.

To explore the ability of **41** to interfere with the activity of other thermo-TRP ion channels, namely TRPM8 and TRPA1, **41** was also tested in patch-clamp experiments in HEK cells stably expressing human transient receptor potential cation channel subfamily M member 8 (hTRPM8) or human transient receptor potential cation channel subfamily A member 1 (hTRPA1) channels. In these experiments, WS12 at 1 μM and AITC at 60 μM were used as agonists of TRPM8 and TRPA1, respectively. As depicted in Fig. 5A, 100 μM **41** was able to activate both ion channels, although to a lower extent than the canonical agonists (Fig. 5A,C). Moreover, the activation of both ion channels by **41** is blocked by the respective antagonist of TRPM8 (AMTB) or TRPA1

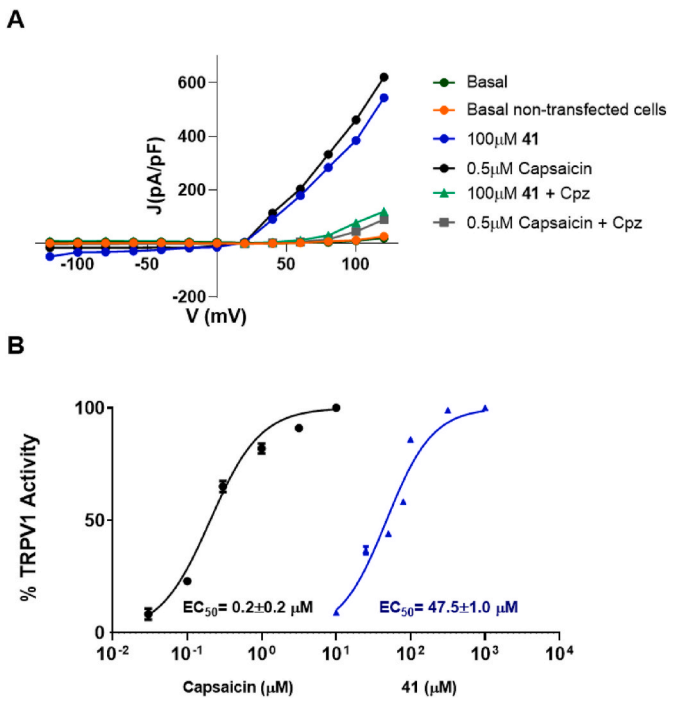

Fig. 3. Electrophysiological evaluation of **41** on heterologously expressed hTRPV1 channel. (A) Representative traces of currents evoked by a 100 ms voltage ramp ranging from −120 mV to +120 mV applied every 4 s in control solution (dark green trace), during application of capsaicin 0.5 μM (black trace) or 100 μM **41** (blue trace) or in non-transfected cells (orange trace) or in the presence of capsazepine 1 μM and capsaicin 0.5 μM (gray curve) or capsazepine 1 μM and **41** 100 μM (light green curve). Peak current data represented were expressed as pA/pF (to allow comparison among different size cells). (B) Capsaicin and **41** dose-response curves. Data were fitted to a non-linear fit curve of log(agonist): Y = 100/(1 + 10^((LogEC$_{50}$-X)*HillSlope)). The best fit for capsaicin provided an EC$_{50}$ value of 0.2 (95 % CI 0.2–0.35) μM and Hill coefficient was 1.3 (95 % CI 0.8–1.7). EC$_{50}$ for **41** was 47.5 (95 % CI 40.3–56) μM and Hill coefficient was 1.4 (1–1.77) (n = 5–10).

(HC030031), indicating the specific effect of **41** on these channels (Fig. 5 A,C, black traces). Quantification of **41** agonism shows the compound capability to activate both channels by ≈ 25 % (Fig. 5B,D), indicating a good level of selectivity of **41** for TRPV1 over TRPM8 and TRPA1.

2.5. Molecular modeling of the interaction between 41 and TRPV1 channel or CB2 receptor

Computational studies were performed to investigate the possible binding mode of compound **41** to both TRPV1 and CB2 proteins.

With regard to TRPV1, docking studies were accomplished using the three-dimensional structure of human TRPV1 at 2.29 Å resolution (PDB ID: 8GFA) [7]. Capsaicin binding site was located by superimposing the human TRPV1 with the squirrel TRPV1 structure (3.81 Å resolution), determined in complex with capsaicin (PDB ID: 7LR0) [62]. To explore binding modes of compound **41** the activated human CB2 receptor (PDB ID: 6KPF) [63], determined by cryo-electron microscopy at 2.90 Å resolution, was used. This structure of CB2 in complex with the agonist AM12033 (Ki = 0.37 nM for CB2) was selected based on its reliability and stability.

The starting conformation of compound **41** was obtained by minimization. Then, series of docking simulations with the software implemented in Yasara were ran to investigate whether the TRPV1 tetramer or CB2 receptor was able to bind **41**, limiting the search space to a simulation box built 5 Å around the well-known ligands (capsaicin and AM12033 for TRPV1 and CB2, respectively) (Fig. 6A and 7A). A total of 500 flexible docking runs were set and clustered around the selected binding sites.

Fig. 6B shows the detail of the capsaicin binding pocket with bound capsaicin (wheat color) or compound **41** (blue). The hydrocarbon tail of both ligands fits into a binding pocket located between the S4, S4–S5 linker segments of one subunit, and the S6 TM segment of the adjacent subunits. Capsaicin (wheat color) interactions were mainly hydrophobic in the hydrocarbon tail, and polar/hydrophobic in the vanillyl group. In addition, a pi-stacking interaction is observed between Y511 and the vanilloid ring (Fig. 6C). The net of hydrogen bonds (HBs) observed in capsaicin interaction is lost when **41** binds to TRPV1 (Fig. 6D), being the residue N551 the one establishing HBs with the polar end of **41**. The theoretical energies of binding between the ligands and the TRPV1 receptor were evaluated obtaining a value of 8.29 kcal/mol, for capsaicin and 6.68 kcal/mol for **41**. The decrease in the binding energy is due to the lowering of both hydrophobic and HBs interactions observed for **41** with respect to capsaicin. The different binding energy could explain the differences observed in their potency, being capsaicin the more potent.

Fig. 7B shows the detail of the AM12033 binding pocket bound to AM12033 (PDB ID: 6KPF) (wheat color) or compound **41** (blue). The binding pocket located between the S2–S3–S5–S6–S7 segments is capable of harboring both ligands. AM12033 (wheat color) forms mainly hydrophobic and aromatic interactions with the receptor, except for a single HB between the phenolic hydroxyl at C1 of the ligand with S285 residue (Fig. 7C). The HB observed in AM12033 binding is lost when **41** binds to CB2 (Fig. 7D), establishing polar contacts with the residue T114 in a different location of the binding pocket. The theoretical energies of binding between the ligands and the receptor 11.72 kcal/mol for AM12033 and 6.69 kcal/mol for **41** could explain the differences observed in their potency, being the AM12033 the more potent with a Ki = 0.37 nM for CB2.

3. Conclusions

Our previous discovery of Passerini adducts as effective soft drugs for the topical treatment of inflammatory skin disorders[52] inspired us to investigate this strategy to target the cross-talk between the TRPV1 channel and CB1 and CB2 receptors in the search for novel and safer anti-inflammatory and analgesic agents. Except for few examples, the hybrid vanilloid/cannabinoid compounds reported so far, especially the natural mediators, suffer from low potency, poor drug-likeness mainly due to high lipophilicity, not well-balanced activity on CB receptors and TRPV1, promiscuity with variable activities on other related targets (*e.g.*, TRPA1, TRPM8, TRPV4, GPCRs), as well as poor synthetic accessibility.

Taking advantage from its three points of diversity and its ability to afford a variable metabolic stability [52], we applied the Passerini reaction to access high chemical diversity in the preparation of libraries of α-acyloxycarboxamides as soft and hard TRPV1/CB dual modulators. By combining the polar headgroups of endovanilloids, such as AEA, NADA and OLDA, as well as of other CB2/TRPV1 ligands and CB2 inverse agonists, with a pool of fatty chains, we discovered modulators with a diversified biological profile and a finely tunable metabolic stability.

Among those molecules bearing an aliphatic head, three compounds characterized by a soft nature were identified: **54**, endowed with a well-balanced agonism on TRPV1 (EC$_{50}$ = 20.3 μM) and CB1 (EC$_{50}$ = 13.8 μM), **40**, a quite balanced TRPV1/CB1 agonist (TRPV1: EC$_{50}$ = 2.1 μM; CB1: EC$_{50}$ = 30.6 μM), and **51**, more active on TRPV1 than CB2 (TRPV1: EC$_{50}$ = 1.7 μM; CB2: EC$_{50}$ = 87.6 μM). Among those compounds bearing an aromatic head, given the presence of an iodine at position 6, **29** emerged as a TRPV1 antagonist (IC$_{50}$ = 54.2 μM) with a lower CB2 agonist activity (EC$_{50}$ > 100 μM) and poor metabolic stability. Interestingly, **34**, a soft TRPV1 antagonist (IC$_{50}$ = 9.8 μM), also exhibits an indirect agonism on both CB1 and CB2 receptors putatively due to the inhibition of adenylate cyclase (IC$_{50}$ = 40.5 μM).

Due to the paucity of TRPV1/CB2 agonists in the literature and the absence of CB1-mediated psychoactive effects, we focused on **41**, a

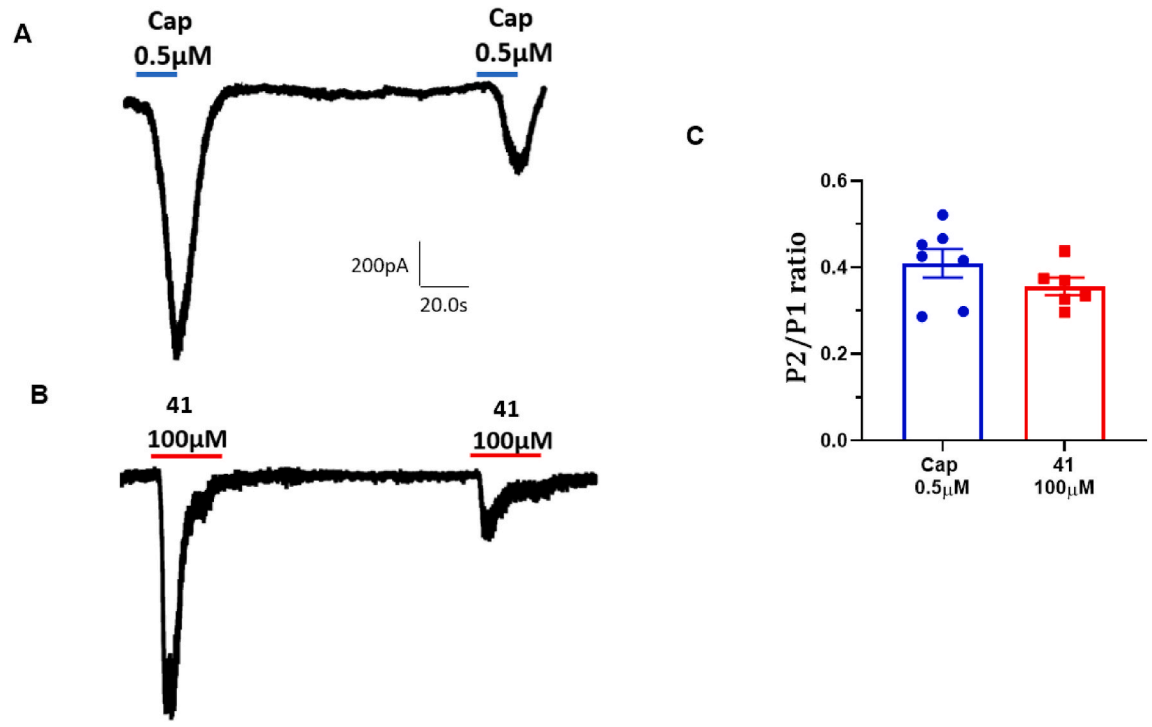

Fig. 4. Electrophysiological evaluation of **41** desensitization capacity on heterologously expressed hTRPV1 channel. (A, B) Representative capsaicin-evoked hTRPV1 current recorded at a holding potential of −60 mV for cells exposed to two capsaicin pulses (0.5 μM) (n = 7) (A), or to two **41** pulses (100 μM) (n = 6) (B), interspersed by a washing period. Horizontal lines denote the duration of compound pulse. (C) P2/P1 ratio represents the current induced by the second pulse of agonist normalized to the first pulse. All data are expressed as mean ± SD. N = 3; n = 8.

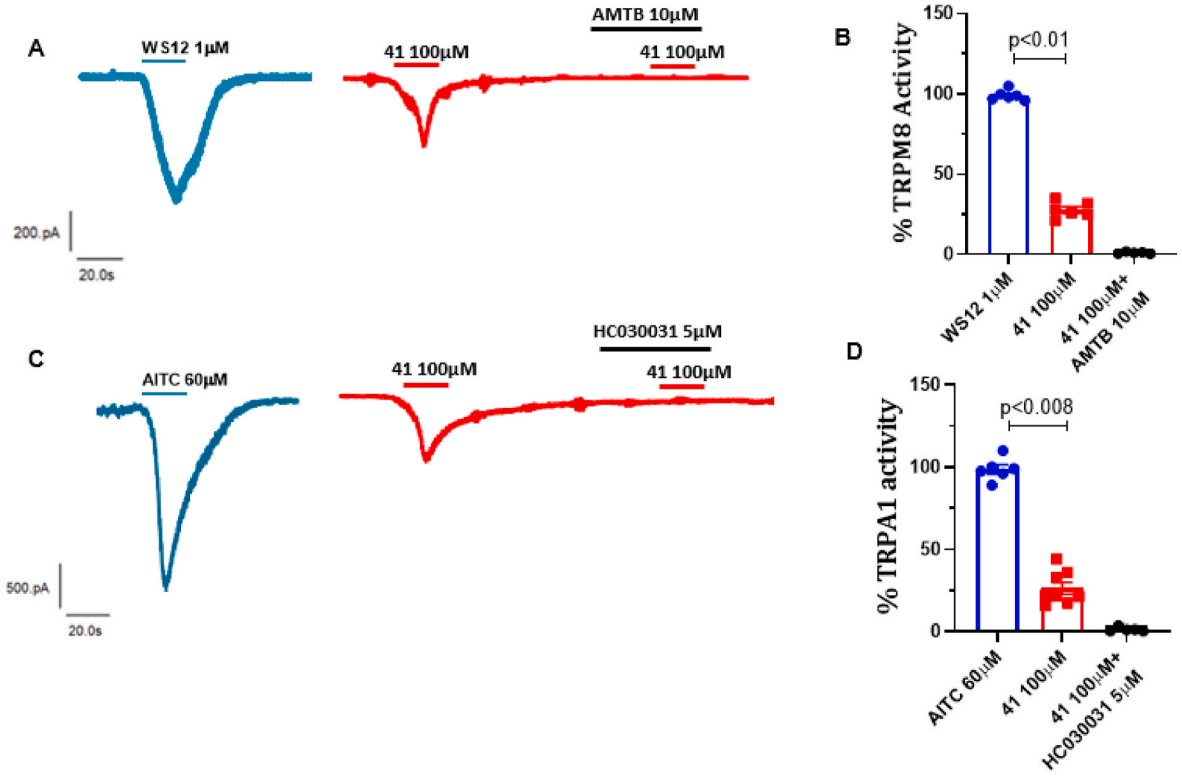

Fig. 5. **41** selectivity over Thermo-TRPs ion channels. (A) Representative 1 μM WS12 (blue line) or 100 μM **41** alone (red line) or in the presence of 10 μM AMTB (black line), elicited hTRPM8 inward currents recorded at a holding potential of −60 mV. (B) Comparison of 1 μM WS12 activation of hTRPM8 and 100 μM **41**. (C) Representative 60 μM AITC (blue line) or 100 μM **41** alone (red line) or in the presence of 10 μM HC030031 (black line), elicited hTRPA1 inward currents recorded at a holding potential of −60 mV. (D) Comparison of 60 μM AITC activation of hTRPA1 and 100 μM **41**. Data were analysed using the non-parametric *t*-test Student, p-values for statistical differences are indicated. All data are expressed as mean ± SEM. N = 3; n = 6–8.

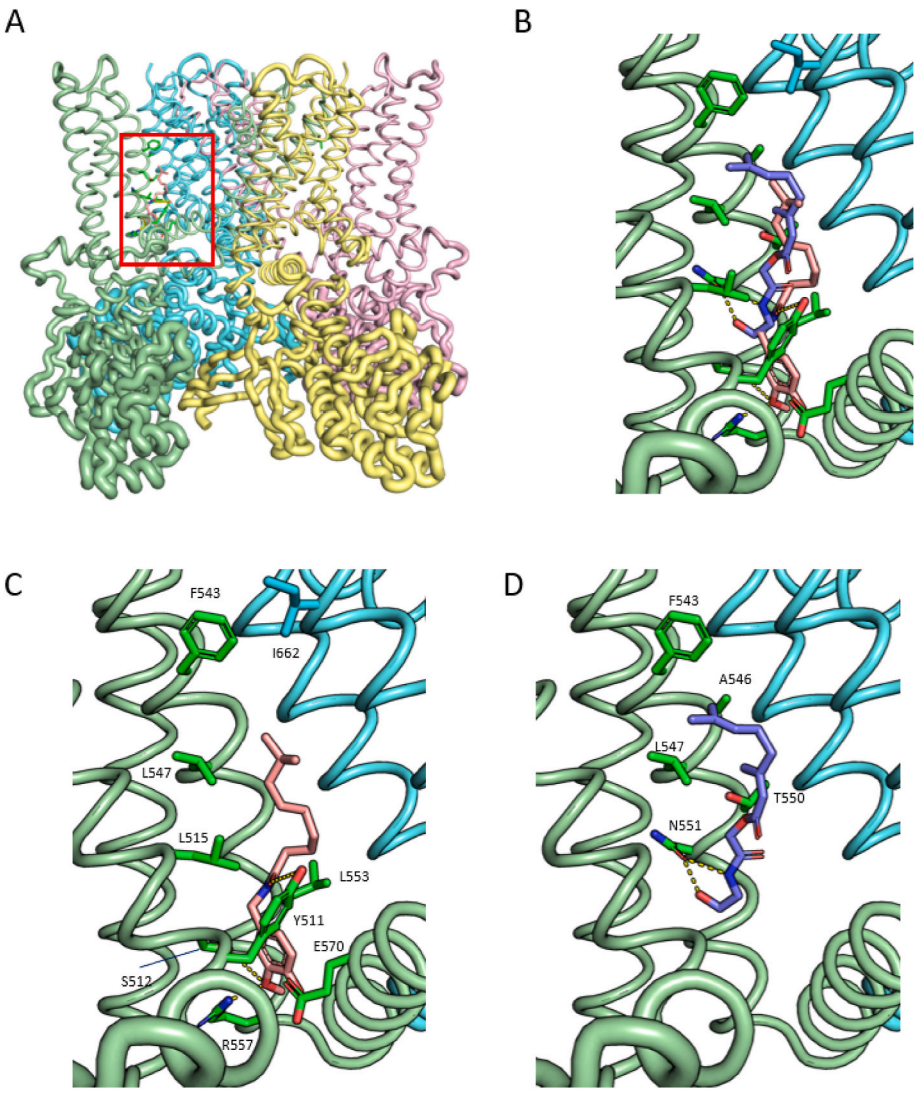

Fig. 6. A) Human TRPV1 structure (PDB ID: 8GFA) is used directly for docking studies. The red square roughly indicates the simulation box built 5 Å around capsaicin binding site to accommodate compound **41**. B) Detail of the capsaicin binding pocket with bound capsaicin (wheat color) or compound **41** (blue) superimposed for comparison. C) Capsaicin (wheat color) interactions. Residues mainly involved in hydrophobic interactions are L515, F543, L547, L553, and E570 (green, chain A), and I662 (cyan, chain B), while HBs (yellow dotted lines) are formed between Y511, S512, R557, E570, and the vanillyl group. In addition, a pi-stacking interaction is observed between Y511 and the vanilloid ring. D) The compound **41** (blue color) interacts directly with a few hydrophobic residues (F543, A546, L547, and T550).

compound that bears the ethanolamine substructure in the head and the geranyl substructure in the tail, and showed an exquisite metabolic stability in all the tested settings compatible with a systemic use and a well-balanced agonism on TRPV1 (EC_{50} = 26.8 μM) and CB2 (EC_{50} = 37.8 μM). In patch-clamp assays, it showed similar efficacy, albeit less potency, when compared to capsaicin in activating heterologously expressed hTRPV1 and in inducing channel desensitization. Moreover, in additional patch-clamp experiments aimed at assessing the selectivity for hTRPV1, **41** shows a high degree of selectivity over hTRPM8 and hTRPA1. Docking simulations allowed to predict **41** binding poses at both the capsaicin-binding site of hTRPV1 and the orthosteric pocket of hCB2.

In conclusion, by capitalizing on a diversity-oriented approach, our work resulted in the discovery of single targeting as well as dual targeting compounds, some of them taking shape as soft drugs for topical use and some others as hard drugs for systemic administration. Among them, we identified a novel TRPV1/CB2 dual agonist, **41**, endowed with high synthetic feasibility, optimal chemical and metabolic stability and low promiscuity, paving the way towards novel therapeutic options for the treatment of pain and inflammatory disorders. Other compounds reported in our study also present interesting profiles and might serve as chemical probes to be used in the future to better elucidate the still poorly understood function of the EV/EC system.

4. Experimental section

Chemistry. Commercially available reagents and solvents were used as purchased without further purification. When needed, solvents were distilled and stored on molecular sieves. Reactions were monitored by thin layer chromatography (TLC) carried out on 5 cm × 20 cm silica gel plates with a layer thickness of 0.25 mm, using UV light as a visualizing agent. When necessary, TLC plates were visualized with aqueous $KMnO_4$.

Column chromatography was performed on flash silica gel using Kieselgel 60 silica gel (particle size 0.040−0.063 mm, 230−400 mesh). Melting points were determined in open glass capillary with a Stuart scientific SMP3 apparatus. All the target compounds were checked by IR (FT-IR Bruker Alpha II), ^{1}H NMR and ^{13}C NMR (Jeol ECP 300 MHz and

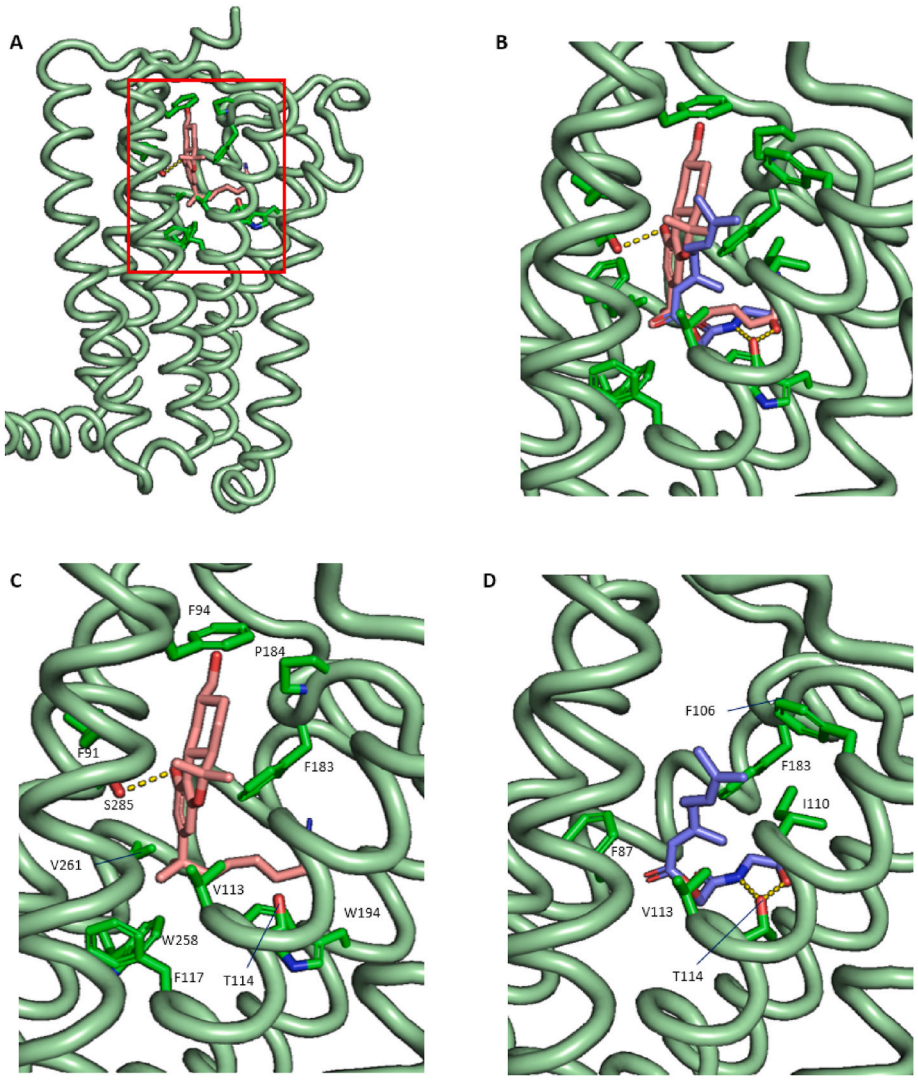

Fig. 7. A) Human CB2 receptor in complex with the agonist AM12033 (PDB ID: 6KPF); the red square roughly indicates the simulation box built 5 Å around the AM12033 to accommodate compound **41**. B) Detail of the AM12033 binding pocket with bound AM12033 (wheat color) or compound **41** (blue) superimposed for comparison. C) AM12033 (wheat color) interactions are mainly hydrophobic, except for a single HB. Residues involved in hydrophobic interactions were F91, F94, V113, T114, F117, F183, P184, W194, W258, and V261 (green). The HBs involved S285 (yellow dotted lines). D) **41** (blue color) interacts directly with less hydrophobic residues (F87, F106, I110, V113, and F183). The HBs observed in AM10233 is changed to residue T114 in a different location in the binding pocket.

Bruker Avance Neo 400 MHz), HRMS (Thermo Fisher Q-Exactive Plus) equipped with an Orbitrap (ion trap) mass analyzer. Chemical shifts are reported in parts per million (ppm) with residual solvent signals as internal standard ($CDCl_3$, $\delta = 7.26$ ppm for ^{1}H NMR, $\delta = 77.16$ ppm for ^{13}C NMR; CD_3OD, $\delta = 3.31$ ppm for ^{1}H NMR, $\delta = 49.00$ ppm for ^{13}C NMR; $(CD_3)_2CO$, $\delta = 2.05$ ppm for ^{1}H NMR, $\delta = 29.84$ and 206.26 ppm for ^{13}C NMR). Coupling constants (*J*) are quoted in Hz. Abbreviations used for multiplicity are as follows: s – singlet, d – doublet, t – triplet, q – quartet, quint – quintet, sext – sextet, dd – doublet of doublets, dt – doublet of triplets, br – broad, m – multiplet.

The purity of selected compounds was determined by HPLC using a Shimadzu HPLC system (Shimadzu, Kyoto, Japan) equipped with a Kinetex C18 (150 × 4.6 mm, 5 μm d.p., Phenomenex Torrance, CA, USA) and using water and acetonitrile as eluents (see chromatograms in the SI). The purity of all tested compounds is 95 % or higher.

4.1. NADA and OLDA analogues

2-(3,4-Bis((*tert*-butyldimethylsilyl)oxy)phenyl)ethan-1-amine. To a suspension of 2-(3,4-dihydroxyphenyl)ethanaminium chloride **3** (5.00 g, 26.37 mmol) in dry CH_2Cl_2 (50 mL), imidazole (3.59 g, 52.74 mmol) was added in one portion under a nitrogen atmosphere. A solution of TBDMSCl (7.95 g, 52.74 mmol) in dry CH_2Cl_2 (25 mL) was added dropwise to the above solution, and the resulting mixture was stirred at room temperature overnight. The volatile was then removed under *vacuum* to obtain a sticky solid, which was solubilized in Et_2O. The organic layer was washed with an aqueous solution of citric acid (10 % w/v), dried over sodium sulfate and evaporated. Purification by column chromatography using EtOAc and EtOAc/CH_3OH 8:2 as eluents yielded title compound as a white solid (5.89 g, 15.42 mmol, 59 %). Mp 78.1–78.6 °C. ^{1}H NMR (300 MHz, $CDCl_3$): $\delta = 8.34$ (br s, 2H), 6.74–6.67 (m, 3H), 3.19 (quint, $J = 6.8$ Hz, 2H), 2.99 (t, $J = 6.8$ Hz, 2H), 1.04–0.76 (m, 18H), 0.25–0.17 (m, 12H). ^{13}C NMR (75 MHz, $CDCl_3$): $\delta = 147.0$, 146.0, 129.3, 121.7, 121.6, 121.3, 41.4, 33.1, 25.9 (4C), 18.4 (2C), −4.1 (2C). IR (neat): $\tilde{\nu} = 2928$, 2857, 1510, 1252, 1125, 984, 902, 777, 663, 460 cm^{-1}. MS (ESI): *m/z* 382 $[M+H]^+$.

***N*-(3,4-Bis((*tert*-butyldimethylsilyl)oxy)phenethyl)formamide (4).** 2-(3,4-Bis((*tert*-butyldimethylsilyl)oxy)phenyl)ethan-1-amine (2.72 g, 7.14 mmol) was dissolved in 1:1 solution of methyl formate and methanol (115 mL) and K_2CO_3 (9.87 g, 71.39 mmol) was added. The

reaction was stirred at reflux for 2h. Then, the reaction was filtered and rinsed with methanol. The volatile was removed under *vacuum* and water was added. The aqueous layer was extracted with CH_2Cl_2 (x2) and the organic phases were collected and dried over sodium sulfate. After evaporation, compound **4** was afforded as a pale-yellow oil (2.55 g, 6.22 mmol, 87 %). ^{1}H NMR (300 MHz, $CDCl_3$, *referred to the main rotamer): δ = 8.12 (s, 1H), 6.76 (d, J = 3.1 Hz, 1H), 6.64–6.61 (m, 2H), 5.48 (br s, 1H), 3.51 (q, J = 6.3 Hz, 2H), 2.70 (t, J = 6.3 Hz, 2H), 1.02–0.98 (m, 18H), 0.26–0.14 (m, 12H). ^{13}C NMR (75 MHz, $CDCl_3$-d_6): δ = 161.1, 146.8, 145.6, 129.8, 121.6, 121.5, 121.1, 39.3, 34.8, 25.9 (4C), 18.4 (2C), −4.1 (2C). IR (neat): $\tilde{\nu}$ = 2929, 2857, 1662, 1509, 1252, 1126, 904, 780, 666, 449 cm^{-1}. MS (ESI): *m/z* 432 $[M+Na]^+$.

((4-(2-Isocyanoethyl)-1,2-phenylene)bis(oxy))bis(tert-butyldimethylsilane) (5). To a solution of *N*-(3,4-bis((*tert*-butyldimethylsilyl)oxy)phenethyl)formamide **4** (2.53 g, 6.18 mmol) in dry CH_2Cl_2 (25 mL), TEA (4.31 mL, 30.91 mmol) was added under nitrogen and the resulting mixture was cooled down at 0 °C. A solution of $POCl_3$ (849 μL, 9.27 mmol) in dry CH_2Cl_2 (15 mL) was added dropwise and the resulting mixture was stirred for 1h at 0 °C. The reaction mixture was quenched with saturated aqueous $NaHCO_3$ solution (40 mL) and stirred for additional 10 min. Then, the two phases were separated and the organic layer was washed with saturated aqueous $NaHCO_3$ solution, dried over sodium sulfate and evaporated. Purification by column chromatography using PE/EtOAc 9:1 as eluent afforded isocyanide **5** (1.87 g, 4.76 mmol, 77 %) as a pale-yellow oil. ^{1}H NMR (300 MHz, $CDCl_3$): δ = 6.78 (d, J = 3.1 Hz, 1H), 6.69–6.67 (m, 2H), 3.54 (t, J = 6.2 Hz, 2H), 2.86 (t, J = 6.2 Hz, 2H), 1.00–0.99 (m, 18H), 0.24–0.20 (m, 12H). ^{13}C NMR (300 MHz, $CDCl_3$): δ = 156.6, 147.0, 146.2, 129.9, 121.6 (2C), 121.3, 43.2, 35.2, 26.0 (4C), 18.5 (2C), −3.9, −4.0. IR (neat): 2930, 2858, 2145, 1511, 1297, 1253, 903, 835, 779 cm^{-1}.

4.1.1. General procedure for the synthesis of compounds 22-28

To a solution of isocyanide **5** (283 mg, 0.72 mmol) in CH_2Cl_2 (6 mL), 37 % aqueous formaldehyde solution (215 μL, 2.88 mmol) and carboxylic acid (0.72 mmol) were added and the resulting mixture was stirred at 40 °C for 3h. Then, the volatile was removed under *vacuum*, obtaining a residue, which was solubilized in THF (6.5 mL) and was cooled down to 0 °C. Acetic acid (145 μL, 2.45 mmol) and TBAF (1 M solution in THF, 2.45 mmol) were added at the same temperature. The ice bath was removed and the reaction mixture was allowed to stirred for 2h at room temperature. The volatile was evaporated; the obtained residue was dissolved in ethyl acetate, washed with water (x1) and then with a saturated aqueous $NaHCO_3$ solution (x1). The collected organic layers were dried over sodium sulfate and evaporated under reduced pressure. Purification by column chromatography yielded compounds **22**–**28**.

2-((3,4-Dihydroxyphenethyl)amino)-2-oxoethyl octanoate (22). Yellow oil (121.5 mg, 0.36 mmol, 50 % yield). Eluent: PE/EtOAc 5:5. ^{1}H NMR (300 MHz, $CDCl_3$): δ = 6.78 (d, J = 8.0 Hz, 1H), 6.69 (s, 1H), 6.51 (d, J = 8.0 Hz, 1H), 6.44 (br s, 1H), 4.52 (s, 2H), 3.46 (q, J = 6.0 Hz, 2H), 2.66 (t, J = 6.3 Hz, 2H), 2.31 (t, J = 6.3 Hz, 2H), 1.57 (quint, J = 6.0 Hz, 2H), 1.27–1.24 (m, 8H), 0.86 (t, J = 6.0 Hz, 3H). ^{13}C NMR (75 MHz, $CDCl_3$): δ = 172.8, 168.4, 144.4, 143.2, 130.4, 120.7, 115.7, 115.5, 62.6, 40.7, 34.7, 33.9, 31.7, 29.8, 29.1, 24.8, 22.7, 14.2. IR (KBr): $\tilde{\nu}$ = 3646, 3267, 2926, 1742, 1659, 1533, 1451, 1281, 1018, 806 cm^{-1}. MS (ESI): *m/z* 360 $[M+Na]^+$.

2-((3,4-Dihydroxyphenethyl)amino)-2-oxoethyl dodecanoate (23). Pale yellow oil (232.3 mg, 0.59 mmol, 82 % yield). PE/EtOAc 5:5. ^{1}H NMR (300 MHz, $CDCl_3$): δ = 6.79 (d, J = 8.0 Hz, 1H), 6.69 (s, 1H), 6.55 (d, J = 8.0 Hz, 1H), 6.25 (br s, 1H), 4.52 (s, 2H), 3.49 (q, J = 6.3 Hz, 2H), 2.69 (t, J = 6.3 Hz, 2H), 2.32 (t, J = 7.4 Hz, 2H), 1.58–1.55 (m, 2H), 1.24–1.15 (m, 16H), 0.86 (t, J = 7.4 Hz, 3H). ^{13}C NMR (75 MHz, $CDCl_3$): δ = 172.9, 168.4, 144.4, 143.2, 130.4, 120.7, 115.8, 115.6, 62.6, 40.8, 34.7, 33.9, 32.0, 29.7 (2C), 29.6, 29.4, 29.3, 29.2, 24.8, 22.8, 14.2. IR (KBr): $\tilde{\nu}$ = 3507, 3386, 2914, 1736, 1658, 1534, 1451, 1282, 1102, 808 cm^{-1}. MS (ESI): *m/z* 394 $[M+H]^+$.

(*R*,*Z*)-2-((3,4-Dihydroxyphenethyl)amino)-2-oxoethyl 12-(2-phenylacetoxy)octadec-9-enoate (24). Colorless oil (193.2 mg, 0.32 mmol, 44 % yield). Eluent: PE/EtOAc 7:3. ^{1}H NMR (300 MHz, $CDCl_3$): δ = 7.28–7.25 (m, 5H), 6.78 (d, J = 7.1 Hz, 1H), 6.69 (s, 1H), 6.56 (d, J = 7.1 Hz, 1H), 6.19 (br s, 1H), 5.44 (q, J = 6.3 Hz, 1H), 5.29 (q, J = 6.3 Hz, 1H), 4.87 (t, J = 6.0 Hz, 1H), 4.53 (s, 2H), 3.60 (s, 2H), 3.51 (q, J = 6.6 Hz, 2H), 2.70 (t, J = 6.6 Hz, 2H), 2.34–2.29 (m, 4H), 2.00 (q, J = 6.3 Hz, 2H), 1.60–1.55 (m, 4H), 1.29–1.22 (m, 16H), 0.87 (t, J = 6.0 Hz, 3H). ^{13}C NMR (75 MHz, $CDCl_3$): δ = 172.4, 171.8, 167.9, 144.5, 143.2, 132.7 (2C), 130.5, 129.3, 128.6, 127.1, 124.2, 120.6, 115.7, 115.5, 74.9, 62.7, 41.9, 40.5, 34.7, 33.9, 33.6, 32.0, 31.8, 31.7, 29.5, 29.2, 29.1, 27.3, 25.4, 25.2, 24.8, 22.6, 14.1. IR (KBr): $\tilde{\nu}$ = 3356, 2925, 2854, 1732, 1658, 1524, 1453, 1259, 1021, 800 cm^{-1}. MS (ESI): *m/z* 632 $[M+Na]^+$.

2-((3,4-Dihydroxyphenethyl)amino)-2-oxoethyl oleate (25). Yellow solid (229.6 mg, 0.48 mmol, 67 % yield). Eluent: PE/EtOAc 7:3. Mp 59–60 °C. ^{1}H NMR (300 MHz, $CDCl_3$): δ = 7.03 (br s, 1H), 6.81 (d, J = 7.7 Hz, 1H), 6.69 (d, J = 1.8, 1H), 6.57 (dd, J_s = 7.7 Hz, 1.8 Hz, 1H), 6.25 (br s, 1H), 6.10 (br s, 1H), 5.35–5.32 (m, 2H), 4.54 (s, 2H), 3.52 (q, J = 6.9 Hz, 2H), 2.70 (t, J = 6.9 Hz, 2H), 2.33 (t, J = 7.4 Hz, 2H), 2.04–1.99 (m, 4H), 1.59 (quint, J = 7.4 Hz, 2H), 1.29–1.21 (m, 20H), 0.87 (t, J = 6.6 Hz, 3H). ^{13}C NMR (75 MHz, $CDCl_3$): δ = 172.9, 168.4, 144.4, 143.2, 130.5, 130.1, 129.7, 120.6, 115.8, 115.6, 62.6, 40.8 (2C), 34.6, 33.9, 32.0, 29.8 (2C), 29.6, 29.4, 29.3, 29.2, 29.1, 27.3 (2C), 24.8, 22.7, 14.2. IR (KBr): $\tilde{\nu}$ = 3499, 3384, 2922, 1741, 1658, 1533, 1450, 1257, 804 cm^{-1}. MS (ESI): *m/z* 498 $[M+Na]^+$.

2-((3,4-Dihydroxyphenethyl)amino)-2-oxoethyl (5*Z*,8*Z*,11*Z*,14*Z*)-icosa-5,8,11,14-tetraenoate (26). Pale yellow oil (233.1 mg, 0.47 mmol, 65 % yield). Eluent: PE/EtOAc 7:3. ^{1}H NMR (300 MHz, $CDCl_3$): δ = 6.80 (d, J = 6.9 Hz, 1H), 6.69 (d, J = 1.6 Hz, 1H), 6.56 (dd, J_s = 6.9 and 1.6 Hz, 1H), 6.26 (br s, 1H), 5.39–5.35 (m, 8H), 4.54 (s, 2H), 3.50 (q, J = 6.8 Hz, 2H), 2.84–2.81 (m, 6-[-H), 2.70 (t, J = 6.8 Hz, 2H), 2.35 (t, J = 7.4 Hz, 2H), 2.14–2.01 (m, 4H), 1.67 (quint, J = 7.4 Hz, 2H), 1.37–1.28 (m, 6H), 0.88 (t, J = 6.9 Hz, 3H). ^{13}C NMR (75 MHz, $CDCl_3$): δ = 172.6, 168.3, 144.4, 143.2, 130.6, 130.4, 129.3, 128.7 (2C), 128.4, 128.1, 127.9, 127.6, 120.7, 115.7, 115.6, 62.7, 40.7, 34.7, 33.3, 31.6, 29.4, 27.3, 26.5, 25.8 (3C), 24.6, 22.7, 14.2. IR (neat): $\tilde{\nu}$ = 3352, 3012, 2927, 1744, 1658, 1282, 1146, 912, 876 cm^{-1}. MS (ESI): *m/z* 496 $[M-H]^-$.

2-((3,4-Dihydroxyphenethyl)amino)-2-oxoethyl (*E*)-3,7-dimethylocta-2,6-dienoate (27). Colorless oil (137.7 mg, 0.38 mmol, 53 % yield). Eluent: PE/EtOAc 6.5:3.5. ^{1}H NMR (300 MHz, $CDCl_3$): δ = 6.75 (d, J = 7.6 Hz, 1H), 6.69 (s, 1H), 6.56 (br s, 1H), 6.49 (d, J = 7.6 Hz, 1H), 5.66 (s, 1H), 5.04 (t, J = 6.2 Hz, 1H), 4.54 (s, 2H), 3.44 (t, J = 6.5 Hz, 2H), 2.63 (t, J = 6.5 Hz, 2H), 2.15–2.03 (m, 7H), 1.66 (s, 3H), 1.58 (s, 3H). ^{13}C NMR (75 MHz, $CDCl_3$): δ = 168.7, 165.2, 164.0, 144.4, 143.4, 132.8, 130.5, 122.8, 120.6, 115.7, 115.5, 113.9, 62.1, 41.2, 40.7, 34.7, 26.1, 25.7, 19.2, 17.8. IR (neat): $\tilde{\nu}$ = 3352, 2966, 1722, 1643, 1441, 1371, 1214, 1135, 865, 811 cm^{-1}. MS (ESI): *m/z* 360 $[M-H]^-$.

2-((3,4-Dihydroxyphenethyl)amino)-2-oxoethyl (4*E*,8*E*,12*E*,16*E*)-4,8,13,17,21-pentamethyldocosa-4,8,12,16,20-pentaenoate (28). Yellow oil (77.0 mg, 0.13 mmol, 18 % yield). Eluent: PE/EtOAc 6:4. ^{1}H NMR (300 MHz, $CDCl_3$): δ = 6.79–6.69 (m, 2H), 6.53 (d, J = 6.9 Hz, 1H), 6.34 (br s, 1H), 5.13–5.11 (m, 5H), 4.52 (s, 2H), 3.47 (q, J = 6.9 Hz, 2H), 2.67 (t, J = 6.9 Hz, 2H), 2.45 (t, J = 7.1 Hz, 2H) 2.26 (t, J = 7.1 Hz, 2H), 2.04–1.99 (m, 16H), 1.67–1.59 (m, 18H). ^{13}C NMR (75 MHz, $CDCl_3$): δ = 172.3, 168.1, 144.3, 143.2, 135.3, 135.0, 134.9, 132.9, 131.3, 130.4, 125.7, 124.6, 124.5, 124.3 (2C), 120.7, 115.7, 115.4, 62.7, 40.7, 39.8 (2C), 39.6, 34.7, 34.4, 32.8, 28.3 (2C), 26.9, 26.7 (2C), 25.8, 17.8, 16.1 (2C), 16.1, 15.9. IR (neat): $\tilde{\nu}$ = 3340, 2921, 2853, 1743, 1661, 1443, 1375, 1149, 873, 811 cm^{-1}. MS (ESI): *m/z* 594 $[M+H]^+$.

***N*-(4,5-Bis((*tert*-butyldimethylsilyl)oxy)-2-iodophenethyl)formamide (6).** Intermediate **4** (2.04 g, 4.97 mmol) was solubilized in $CHCl_3$ (20 mL) and silver trifluoroacetate (1.09 g, 4.97 mmol) was added. Iodine (1.26 g, 4.97 mmol) was solubilized in $CHCl_3$ (80 mL) and the resulting violet solution was added dropwise to the reaction at room

temperature. The resulting mixture was stirred for 45 min at room temperature and upon completion was filtered under *vacuum* over a celite pad and rinsed with CH_2Cl_2. The filtrate was washed with saturated aqueous solution of $NaHCO_3$ (x1) and with saturated aqueous $Na_2S_2O_3$ solution (x1). The organic layer was dried over sodium sulfate and evaporated to give compound **6** (2.29 g, 4.27 mmol, 86 %) as a deep yellow oil. ^{1}H NMR (300 MHz, $CDCl_3$, *referred to the main rotamer): δ = 8.15 (s, 1H), 7.25 (s, 1H), 6.67 (s, 1H), 5.58 (br s, 1H), 3.50 (q, J = 6.2 Hz, 2H), 2.82 (t, J = 6.2 Hz, 2H), 1.07–0.90 (m, 18H), 1.18–0.08 (m, 12H). ^{13}C NMR (75 MHz, $CDCl_3$): δ = 161.0, 147.6, 147.4, 133.1, 132.3, 122.4, 87.3, 46.3, 32.2, 26.0 (2C), 25.9 (2C), 18.5 (2C), −4.0, −4.1. IR (neat): $\tilde{\nu}$ = 3284, 2930, 2859, 1663, 1487, 1255, 878, 784, 670 cm^{-1}.

((4-Iodo-5-(2-isocyanoethyl)-1,2-phenylene)bis(oxy))bis(*tert*-butyldimethylsilane) (7). A solution of $POCl_3$ (588 μL, 6.42 mmol) in dry CH_2Cl_2 (10 mL) was added dropwise to a solution of *N*-(4,5-bis((*tert*-butyldimethylsilyl)oxy)-2-iodophenethyl)formamide **6** (2.29 g, 4.28 mmol) and TEA (2.16 mL, 21.41 mmol) in dry CH_2Cl_2 (18 mL) at 0 °C. The reaction mixture was stirred for 1h at the same temperature and then was quenched with a saturated aqueous solution of $NaHCO_3$ (30 mL). The reaction mixture was left to reach room temperature and was stirred for additional 10 min. The two layers were then separated and the organic phase was washed with saturated aqueous $NaHCO_3$ solution (x1), dried over sodium sulfate and evaporated. Purification by column chromatography using PE/EtOAc 9:1 as eluent afforded compound **7** as a white solid (1.82 g, 3.52 mmol, 82 %). Mp: 92–93 °C. ^{1}H NMR (300 MHz, $CDCl_3$): δ = 7.25 (s, 1H), 6.77 (s, 1H), 3.57 (t, J = 6.1 Hz, 2H), 2.96 (t, J = 6.1 Hz, 2H), 1.03–0.93 (m, 18H), 0.21–0.19 (m, 12H). ^{13}C NMR (300 MHz, $CDCl_3$): δ = 157.0, 147.6, 147.2, 132.1, 131.5, 122.8, 88.2, 41.7, 39.7, 26.0 (2C), 25.9 (2C), 18.5 (2C), −3.9, −4.1. IR (KBr): 2930, 2858, 2148, 1553, 1492, 1471, 1379, 843, 779 cm^{-1}.

4.1.2. General procedure for the synthesis of compounds 29–35

To a solution of isocyanide **7** (259.0 mg, 0.50 mmol) in CH_2Cl_2 (4.5 mL), 37 % aqueous formaldehyde solution (150 μL, 2.00 mmol) and carboxylic acid (0.50 mmol) were added and the resulting mixture was stirred at 40 °C for 3h. Then, the volatile was removed under *vacuum* and the crude material was solubilized in THF (4.5 mL). The reaction was cooled to 0 °C and acetic acid (98 μL, 1.70 mmol) and TBAF (1 M solution in THF, 1.70 mmol) were added. The reaction was stirred for 3h at room temperature, then the volatile was removed under *vacuum* and ethyl acetate was added, washed with water (x1) and with saturated aqueous $NaHCO_3$ solution (x1). The organic layer was dried over sodium sulfate and evaporated. Purification by column chromatography yielded compounds **29**–**35**.

2-((4,5-Dihydroxy-2-iodophenethyl)amino)-2-oxoethyl octanoate (29). Brown amorphous solid (155.2 mg, 0.34 mmol, 67 % yield). Eluent: PE/EtOAc 5:5. ^{1}H NMR (400 MHz, $CDCl_3$): δ = 7.30 (s, 1H), 6.75 (s, 1H), 6.38 (br s, 1H), 4.56 (s, 2H), 3.52 (t, J = 6.4 Hz, 2H), 2.84 (t, J = 6.7 Hz, 2H), 2.38 (t, J = 7.6 Hz, 2H), 1.61 (quint, J = 7.5 Hz, 2H), 1.32–1.25 (m, 8H), 0.88 (t, J = 7.2 Hz, 3H). ^{13}C NMR (101 MHz, $CDCl_3$): δ = 172.9, 168.5, 144.7, 144.5, 132.6, 125.4, 116.7, 87.4, 62.7, 39.8, 39.0, 34.1, 31.2, 29.2, 29.0, 24.9, 22.7, 14.2. IR (KBr): $\tilde{\nu}$ = 3525, 3443, 2921, 2362, 1735, 1541, 1459, 1161, 970, 541 cm^{-1}. MS (ESI): *m/z* 464 [M+H]$^+$.

2-((4,5-Dihydroxy-2-iodophenethyl)amino)-2-oxoethyl dodecanoate (30). Yellow oil (181.8 mg, 0.35 mmol, 70 % yield). Eluent: PE/EtOAc 5:5. ^{1}H NMR (300 MHz, $CDCl_3$): δ = 7.30 (s, 1H), 6.74 (s, 1H), 6.32 (br s, 1H), 4.56 (s, 2H), 3.52 (q, J = 6.3 Hz, 2H), 2.85 (t, J = 6.3 Hz, 2H), 2.38 (t, J = 7.4 Hz, 2H), 1.60 (quint, J = 7.4 Hz, 2H), 1.25–1.17 (m, 16H), 0.89 (t, J = 6.9 Hz, 3H).^{13}C NMR (75 MHz, $CDCl_3$): δ = 172.9, 168.7, 145.0, 144.4, 132.6, 125.6, 116.6, 87.4, 62.7, 39.9, 38.9, 34.0, 32.0, 29.7 (2C), 29.6, 29.4 (2C), 29.2, 24.8, 22.8, 14.2. IR (KBr): $\tilde{\nu}$ = 3394, 2921, 2851, 1735, 1545, 1454, 1274, 1161, 874, 417 cm^{-1}. MS (ESI): *m/z* 518 [M−H]$^-$.

2-((4,5-Dihydroxy-2-iodophenethyl)amino)-2-oxoethyl (*R*,*Z*)-12-(2-phenylacetoxy)octadec-9-enoate (31). Dark yellow oil (147.1 mg, 0.20 mmol, 39 % yield). Eluent: PE/EtOAc 7:3. ^{1}H NMR (300 MHz, $CDCl_3$): δ = 7.28–7.26 (m, 6H), 6.71 (s, 1H), 6.14 (br s, 1H), 5.46–5.44 (m, 1H), 5.31–5.29 (m, 1H), 4.87–4.85 (m, 1H), 4.55 (s, 2H), 3.60–3.53 (m, 4H), 2.85 (t, J = 6.8 Hz, 2H), 2.36–2.28 (m, 4H), 1.99 (t, J = 7.2 Hz, 2H), 1.59–1.53 (m, 4H), 1.28–1.22 (m, 16H), 0.87 (t, J = 6.8 Hz, 3H).^{13}C NMR (75 MHz, $CDCl_3$): δ = 172.5, 171.5, 167.8, 162.9, 145.3, 144.6, 134.4, 132.7, 129.3, 128.5, 127.0, 125.5, 124.2, 116.6, 87.0, 74.7, 62.8, 41.8, 40.0, 39.8, 36.7 (2C), 33.7, 33.6, 32.0, 31.7, 29.5 (2C), 29.1, 27.3, 25.2, 24.8, 22.5, 14.1. IR (KBr): $\tilde{\nu}$ = 3355, 2926, 2855, 2361, 1730, 1659, 1264, 1029, 804, 624 cm^{-1}. MS (ESI): *m/z* 734 [M−H]$^-$.

2-((4,5-Dihydroxy-2-iodophenethyl)amino)-2-oxoethyl oleate (32). Dark yellow oil (183.6 mg, 0.30 mmol, 61 % yield). Eluent: PE/EtOAc 6:4. ^{1}H NMR (300 MHz, $CDCl_3$): δ = 7.30 (s, 1H), 6.75 (s, 1H), 6.36 (br s, 1H), 5.36–5.32 (m, 2H), 4.56 (s, 2H), 3.52 (q, J = 6.8 Hz, 2H), 2.85 (t, J = 6.8 Hz, 2H), 2.38 (t, J = 7.4 Hz, 2H), 2.01–1.99 (m, 4H), 1.61 (quint, J = 7.4 Hz, 2H), 1.29–1.26 (m, 20H), 0.87 (t, J = 7.1 Hz, 3H). ^{13}C NMR (75 MHz, $CDCl_3$): δ = 172.9, 168.7, 145.0, 144.4, 132.6, 130.1, 129.8, 125.6, 116.6, 87.4, 62.7, 39.9, 39.4, 34.0, 32.0, 29.8 (2C), 29.6, 29.4 (2C), 29.3, 29.2 (2C), 27.3 (2C), 24.8, 22.8, 14.2. IR (neat): $\tilde{\nu}$ = 3352, 2923, 2853, 1737, 1655, 1419, 1363, 1154, 874 cm^{-1}. MS (ESI): *m/z* 624 [M+Na]$^+$.

2-((4,5-Dihydroxy-2-iodophenethyl)amino)-2-oxoethyl (5*Z*,8*Z*,11*Z*,14*Z*)-icosa-5,8,11,14-tetraenoate (33). Pale yellow oil (237.1 mg, 0.38 mmol, 76 % yield). Eluent: PE/EtOAc 7:3. ^{1}H NMR (300 MHz, $CDCl_3$): δ = 7.30 (s, 1H), 6.74 (s, 1H), 6.34 (br s, 1H), 5.40–5.36 (m, 8H), 4.56 (s, 2H), 3.51 (q, J = 6.3 Hz, 2H), 2.85–2.80 (m, 8H), 2.40 (t, J = 7.4 Hz, 2H), 2.15–2.01 (m, 4H), 1.70 (quint, J = 7.4 Hz, 2H), 1.37–1.29 (m, 6H), 0.88 (t, J = 6.7 Hz, 3H). ^{13}C NMR (75 MHz, $CDCl_3$): δ = 172.6, 168.7, 145.0, 144.4, 132.6, 130.6, 129.3, 128.7 (2C), 128.5, 128.1, 127.9, 127.6, 125.6, 116.6, 87.4, 62.7, 40.0, 38.9, 33.4, 31.6, 29.4, 27.3, 26.5, 25.7 (3C), 24.6, 22.7, 14.2. IR (neat): $\tilde{\nu}$ = 3348, 3011, 2927, 1743, 1656, 1435, 1144, 876, 709 cm^{-1}. MS (ESI): *m/z* 646 [M+23]$^+$.

2-((4,5-Dihydroxy-2-iodophenethyl)amino)-2-oxoethyl (*E*)-3,7-dimethylocta-2,6-dienoate (34). Yellow solid (104.7 mg, 0.21 mmol, 43 % yield). Eluent: PE/EtOAc 6.5:3.5. Mp 79–80 °C. ^{1}H NMR (400 MHz, $(CD_3)_2CO$): δ = 8.15 (br s, 1H), 7.43 (br s, 1H), 7.26 (s, 1H), 6.83 (s, 1H), 5.77 (q, J = 1.3 Hz, 1H), 5.16–5.11 (m, 1H), 4.53 (s, 2H), 3.51–3.37 (m, 2H), 2.80 (t, J = 7.1 Hz, 2H), 2.24–2.20 (m, 4H), 2.18 (d, J = 1.3 Hz, 3H), 1.69 (s, 3H), 1.63 (s, 3H). ^{13}C NMR (101 MHz, $CDCl_3$): δ = 169.1, 165.2, 164.3, 144.9, 144.6, 133.0, 132.6, 125.4, 122.8, 116.5, 114.0, 87.4, 62.1, 41.3, 39.9, 39.0, 26.1, 25.8, 19.4, 17.9. IR (KBr): $\tilde{\nu}$ = 3507, 3381, 2934, 1712, 1647, 1501, 1389, 1135, 875, 804 cm^{-1}. MS (ESI): *m/z* 486 [M−H]$^-$.

2-((4,5-Dihydroxy-2-iodophenethyl)amino)-2-oxoethyl (4*E*,8*E*,12*E*,16*E*)-4,8,13,17,21-pentamethyldocosa-4,8,12,16,20-pentaenoate (35). Yellow oil (118.8 mg, 0.17 mmol, 33 % yield). Eluent: PE/EtOAc 6:4. ^{1}H NMR (300 MHz, $CDCl_3$): δ = 7.28 (s, 1H), 6.76 (s, 1H), 6.51 (br s, 1H), 5.13–5.09 (m, 5H), 4.56 (s, 2H), 3.48 (q, J = 6.3 Hz, 2H), 2.82 (t, J = 6.3 Hz, 2H), 2.49 (t, J = 7.4 Hz, 2H), 2.28 (t, J = 7.4 Hz, 2H), 2.04–1.99 (m, 16H), 1.67–1.46 (m, 18H). ^{13}C NMR (75 MHz, $CDCl_3$): δ = 172.4, 168.6, 144.9, 144.5, 135.2, 135.0, 134.9, 132.9, 132.5, 131.3, 125.7, 125.5, 124.6, 124.5, 124.3 (2C), 116.6, 87.4, 62.7, 39.9, 39.8 (2C), 39.6, 38.9, 34.4, 32.9, 28.4 (2C), 26.9, 26.8 (2C), 25.8, 17.8, 16.2 (2C), 16.1, 16.0. IR (neat): $\tilde{\nu}$ = 3347, 2926, 2855, 1747, 1660, 1437, 1375, 1148, 875, 841 cm^{-1}. MS (ESI): *m/z* 718 [M−H]$^-$.

4.2. AEA analogues

2-((*tert*-Butyldimethylsilyl)oxy)ethan-1-amine (9). To a solution of ethanolamine **8** (10.00 g, 163.72 mmol) and imidazole (22.30 g, 327.44 mmol) in dry CH_2Cl_2 (164 mL) a solution of TBDMSCl (25.90 g, 171.91 mmol) in dry CH_2Cl_2 (164 mL) was added dropwise under a nitrogen atmosphere. The reaction was stirred for 2h at room temperature. Upon completion, water was added and the reaction was stirred for additional 10 min at the same temperature. The aqueous layer was

extracted with CH_2Cl_2 (x4) and the combined organic phases were dried over sodium sulfate and evaporated under *vacuum*, yielding compound **9** (28.30 g, 161.17 mmol, 98 %) as a dark yellow oil. ^{1}H NMR (300 MHz, $CDCl_3$): $\delta = 3.59$ (t, $J = 6.0$ Hz, 2H), 2.73 (t, $J = 6.0$ Hz, 2H), 2.56 (br s, 2H), 0.86 (s, 9H), 0.01 (s, 6H). ^{13}C NMR (75 MHz, $CDCl_3$): $\delta = 65.0$, 44.2, 25.9, 18.2, −5.4. IR (neat): $\tilde{\nu} = 2953$, 2928, 2856, 1463, 1253, 1100, 903, 833, 775, 663. cm^{-1}. MS (ESI): *m/z* 176 $[M+H]^+$.

***N*-(2-((*tert*-Butyldimethylsilyl)oxy)ethyl)formamide (10).** Anhydrous sodium formate (1.55 g, 22.8 mmol) was suspended in diethyl ether (12 mL) and acetyl chloride (0.89 g, 11.4 mmol) was added and the resulting mixture was stirred overnight. The precipitated was then filtered off and the obtained clear solution was added to a solution of intermediate **9** (1.00 g, 5.70 mmol) in diethyl ether (12 mL) under a nitrogen atmosphere. The reaction was stirred for 5h at room temperature. Then, the volatile was removed under *vacuum* and ethyl acetate was added. The organic layer was washed with water (x3), dried over sodium sulfate and evaporated, yielding compound **10** as a dark yellow oil (0.85 g, 4.17 mmol, 73 %). ^{1}H NMR (300 MHz, $CDCl_3$): $\delta = 8.19$ (s, 1H), 3.71 (t, $J = 6.9$ Hz, 2H), 3.42 (t, $J = 6.9$ Hz, 2H), 0.90 (s, 9H), 0.06 (s, 6H). ^{13}C NMR (75 MHz, $CDCl_3$): $\delta = 161.3$, 61.6, 40.3, 25.8, 18.2, −5.4. IR (neat): $\tilde{\nu} = 3292$, 2929, 2857, 1663, 1471, 1253, 1100, 833, 777, 681 cm^{-1}. MS (ESI): *m/z* 202 $[M-H]^-$.

***tert*-Butyl(2-isocyanoethoxy)dimethylsilane (11).** To a solution of intermediate **10** (0.85 g, 4.17 mmol) in dry CH_2Cl_2 (16 mL) TEA (2.90 mL, 20.85 mmol) was added under a nitrogen atmosphere and the resulting mixture was cooled down to 0 °C. A solution of $POCl_3$ (572 μL, 6.25 mmol) in dry CH_2Cl_2 (10 mL) was added dropwise and the reaction was stirred for 1h at 0 °C. Then, the reaction was quenched with saturated aqueous $NaHCO_3$ solution (26 mL) and stirred for additional 10 min at room temperature. The two phases were separated and the organic layer was washed with a saturated aqueous $NaHCO_3$ solution, dried over sodium sulfate and evaporated, yielding compound **11** (0.77 g, 4.15 mmol, 99 %) as a dark brown oil. ^{1}H NMR (300 MHz, $CDCl_3$): $\delta =$ 3.81–3.77 (m, 2H), 3.49–3.45 (m, 2H), 0.89 (s, 9H), 0.09 (s, 6H). ^{13}C NMR (75 MHz, $CDCl_3$): $\delta = 157.2$, 61.1, 44.1, 35.8, 18.2, −5.4. IR (neat): $\tilde{\nu} = 2929$, 2857, 2149, 1471, 1254, 1123, 931, 834, 776, 662 cm^{-1}. MS (ESI): *m/z* 186 $[M+H]^+$.

4.2.1. General procedure for the synthesis of compounds 36–42

To a solution of intermediate **11** (133.0 mg, 0.72 mmol) in CH_2Cl_2 (6.5 mL), 37 % aqueous formaldehyde solution (215 μL, 2.88 mmol) and carboxylic acid (0.72 mmol) were added and the resulting mixture was stirred at 40 °C for 2h. Then, the volatile was removed under *vacuum* and the obtained residue product was solubilized in THF (6.5 mL) and cooled to 0 °C. At this temperature, acetic acid (49 μL, 0.86 mmol) and TBAF (1 M solution in THF, 0.86 mmol) were added. The resulting reaction mixture was stirred for 2h at room temperature. Upon completion, the volatile was evaporated and ethyl acetate was added, washed with water (x2), dried over sodium sulfate and evaporated. The crude products were purified through column chromatography affording compounds **36**–**42**.

2-((2-Hydroxyethyl)amino)-2-oxoethyl octanoate (36). Colorless oil (71.1 mg, 0.29 mmol, 40 % yield). Eluent: PE/EtOAc 4:6. ^{1}H NMR (300 MHz, $CDCl_3$): $\delta = 4.62$ (s, 2H), 3.76 (t, $J = 4.4$ Hz, 2H), 3.49 (q, $J =$ 4.4 Hz, 2H), 2.42 (t, $J = 6.6$ Hz, 2H), 1.72–1.70 (m, 2H), 1.31–1.29 (m, 8H), 0.89 (t, $J = 6.6$ Hz, 3H).^{13}C NMR (75 MHz, $CDCl_3$): $\delta = 172.6$, 168.3, 62.7, 61.3, 41.9, 33.9, 31.6, 29.0, 28.9, 24.8, 22.5, 14.0. IR (neat): $\tilde{\nu} = 3271$, 2923, 2362, 1736, 1663, 1542, 1261, 1061, 799, 582 cm^{-1}. MS (ESI): *m/z* 268 $[M+Na]^+$.

2-((2-Hydroxyethyl)amino)-2-oxoethyl dodecanoate (37). White solid (105.5 mg, 0.35 mmol, 49 % yield). Eluent: PE/EtOAc 2:8. Mp 73–74 °C. ^{1}H NMR (300 MHz, $CDCl_3$): $\delta = 4.59$ (s, 2H), 3.76 (t, $J = 5.0$ Hz, 2H), 3.50 (q, $J = 5.0$ Hz, 2H), 2.41 (t, $J = 7.7$ Hz, 2H), 1.65 (quint, J = 7.7 Hz, 2H), 1.27–1.23 (m, 16H), 0.87 (t, $J = 6.9$ Hz, 3H). ^{13}C NMR (75 MHz, $CDCl_3$): $\delta = 172.7$, 168.4, 62.8, 61.5, 41.9, 34.0, 32.0, 29.7 (2C), 29.5, 29.4, 29.3, 29.2, 24.9, 22.8, 14.2. IR (neat): $\tilde{\nu} = 3260$, 2953, 2850, 1736, 1642, 1549, 1298, 1062, 776, 579 cm^{-1}. MS (ESI): *m/z* 324 $[M+Na]^+$.

2-((2-Hydroxyethyl)amino)-2-oxoethyl (*R*,*Z*)-12-(2-phenylacetoxy)octadec-9-enoate (38). Colorless oil (72.5 mg, 0.14 mmol, 20 % yield). Eluent: PE/EtOAc 4:6. ^{1}H NMR (300 MHz, $CDCl_3$): $\delta =$ 7.27–7.24 (m, 5H), 6.57 (br s, 1H), 5.39 (q, $J = 6.3$ Hz, 1H), 5.28 (q, $J =$ 6.3 Hz, 1H), 4.93–4.91 (m, 1H), 4.56 (s, 2H), 3.71 (t, $J = 6.6$ Hz, 2H), 3.57 (s, 2H), 3.45 (q, $J = 6.6$ Hz, 2H), 2.40–2.38 (m, 2H), 2.27–2.25 (m, 2H), 2.01–1.99 (m, 4H), 1.71–1.64 (m, 4H), 1.29–1.25 (m, 14H), 0.95 (t, $J = 6.9$ Hz, 3H). ^{13}C NMR (75 MHz, $CDCl_3$): $\delta = 172.4$, 171.6, 168.2, 134.4, 132.8, 129.4, 128.6, 127.1, 124.3, 74.7, 63.0, 62.0, 42.0 (2C), 34.1, 33.7, 32.0, 31.8, 30.0 (2C), 29.2 (3C), 27.4, 25.3, 24.9, 22.7, 14.2. MS (ESI): *m/z* 518 $[M+H]^+$.

2-((2-Hydroxyethyl)amino)-2-oxoethyl oleate (39). White amorphous solid (95.9 mg, 0.25 mmol, 35 % yield). Eluent: PE/EtOAc 2:8. ^{1}H NMR (300 MHz, $CDCl_3$): $\delta = 6.60$ (br s, 1H), 5.33–5.28 (m, 2H), 4.57 (s, 2H), 3.73 (t, $J = 5.0$ Hz, 2H), 3.46 (t, $J = 5.0$ Hz, 2H), 2.61 (br s, 1H), 2.40 (t, $J = 7.4$ Hz, 2H), 2.01–1.93 (m, 4H), 1.65 (t, $J = 7.4$ Hz, 2H), 1.32–1.26 (m, 20H), 0.87 (t, $J = 6.6$ Hz, 3H). ^{13}C NMR (75 MHz, $CDCl_3$): $\delta = 172.4$, 168.2, 130.1, 130.0, 62.8, 61.6, 41.8, 33.9, 31.9, 29.7 (2C), 29.5, 29.3 (2C), 29.1, 29.0 (2C), 27.2, 27.1, 24.8, 22.6, 14.1. IR (neat): $\tilde{\nu}$ = 3274, 2924, 2853, 1732, 1662, 1558, 1466, 1170, 1059, 723 cm^{-1}. MS (ESI): *m/z* 384 $[M+H]^+$.

2-((2-Hydroxyethyl)amino)-2-oxoethyl (5*Z*,8*Z*,11*Z*,14*Z*)-icosa-5,8,11,14-tetraenoate (40). Colorless oil (105.2 mg, 0.26 mmol, 36 % yield). Eluent: PE/EtOAc 6:4. ^{1}H NMR (400 MHz, $CDCl_3$): $\delta = 6.52$ (br s, 1H), 5.46–5.30 (m, 8H), 4.59 (s, 2H), 4.12 (q, $J = 7.2$ Hz, 1H), 3.76 (t, J = 5.0 Hz, 2H), 3.49 (q, $J = 5.4$ Hz, 2H), 2.85–2.80 (m, 6H), 2.43 (t, $J =$ 7.6 Hz, 2H), 2.13 (q, $J = 7.1$ Hz, 2H), 2.08–2.03 (m, 2H), 1.75 (quint, J = 7.2 Hz, 2H), 1.34–1.24 (m, 6H), 0.91–0.87 (m, 3H). ^{13}C NMR (101 MHz, $CDCl_3$): $\delta = 172.2$, 168.2, 130.7, 129.4, 128.8, 128.7, 128.5, 128.2, 127.9, 127.6, 63.0, 62.1, 42.0, 33.4, 31.7, 29.9, 29.5, 27.4, 27.1 26.6, 25.8, 24.7, 22.7, 14.2. IR (neat): $\tilde{\nu} = 3351$, 2926, 1739, 1660, 1549, 1149, 1062, 891 cm^{-1}. MS (ESI): *m/z* 406 $[M+H]^+$.

(*E*)-2-((2-Hydroxyethyl)amino)-2-oxoethyl 3,7-dimethylocta-2,6-dienoate (41). Colorless oil (81.3 mg, 0.30 mmol, 42 % yield). Eluent: PE/EtOAc 4:6. ^{1}H NMR (400 MHz, $(CD_3)_2CO$): $\delta = 7.32$ (s, 1H), 5.78–5.77 (m, 1H), 5.14–5.09 (m, 1H), 4.52 (s, 2H), 3.86 (t, $J = 5.5$ Hz, 1H), 3.59 (q, $J = 5.6$ Hz, 2H), 3.33 (q, $J = 5.7$ Hz, 2H), 2.24–2.18 (m, 4H), 2.17 (d, $J = 1.3$ Hz, 3H), 1.67 (s, 3H), 1.61 (s, 3H). ^{13}C NMR (101 MHz, $CDCl_3$): $\delta = 168.8$, 165.1, 163.7, 132.9, 122.8, 114.1, 62.4, 62.1, 42.1, 41.3, 26.2, 25.8, 19.3, 17.9. IR (neat): $\tilde{\nu} = 3310$, 2924, 1724, 1645, 1546, 1215, 1136, 864 cm^{-1}. MS (ESI): *m/z* 270 $[M+H]^+$.

(4*E*,8*E*,12*E*,16*E*)-2-((2-Hydroxyethyl)amino)-2-oxoethyl 4,8,13,17,21-pentamethyldocosa-4,8,12,16,20-pentaenoate (42). Dark yellow oil (160.6 mg, 0.32 mmol, 44 % yield). Eluent: PE/EtOAc 3:7. ^{1}H NMR (300 MHz, $CDCl_3$): $\delta = 6.55$ (br s, 1H), 5.19–5.08 (m, 5H), 4.57 (s, 2H), 3.75 (t, $J = 5.1$ Hz, 2H), 3.47 (t, $J = 5.2$ Hz, 2H), 2.52 (t, $J =$ 8.1 Hz, 2H), 2.33 (t, $J = 8.1$ Hz, 2H), 2.08–1.74 (m, 16H), 1.90 (s, 3H), 1.67 (s, 3H), 1.62 (s, 3H), 1.59–1.55 (m, 9H). ^{13}C NMR (75 MHz, $CDCl_3$): $\delta = 172.1$, 168.1, 135.0, 134.7, 134.6, 132.7, 131.1, 125.4, 124.3, 124.2, 124.1 (2C), 62.6, 61.2, 41.7, 39.6 (2C), 39.4, 34.2, 32.7, 28.1 (2C), 26.5 (3C), 25.5, 17.5, 15.9 (2C), 15.7 (2C). IR (neat): $\tilde{\nu} = 3368$, 2923, 1741, 1665, 1439, 1376, 1150, 888, 847 cm^{-1}. MS (ESI): *m/z* 524 $[M+Na]^+$.

3-Isocyanoprop-1-ene (13). To an aqueous solution of NaOH (2.07 g, 50 % p/v), a mixture of allylamine **12** (600 mg, 10.51 mmol), $CHCl_3$ (814 μL, 10.09 mmol), triethylbenzylammonium chloride (14.12 mg, 0.062 mmol) and CH_2Cl_2 (2.10 mL) was added dropwise for 20 min under nitrogen atmosphere. The reaction was heated to 45 °C and intensively stirred for 3h. Then, the reaction was extracted with 13.5 mL of CH_2Cl_2 (2x) and the collected organic layers were washed with water (x1). The volatile was evaporated under *vacuum*. ^{1}H NMR (300 MHz, $CDCl_3$): $\delta = 5.74$–5.70 (m, 1H), 5.40–5.32 (m, 1H), 5.24–5.14 (m, 1H), 4.04 (d, $J = 6.3$ Hz, 2H).

4.2.2. General procedure for the synthesis of compounds 43–55

To a solution of intermediate **13** or cyclopropyl isocyanide **14** (0.48 mmol) in CH_2Cl_2 (4.5 mL), 37 % aqueous formaldehyde solution (144 μL, 1.92 mmol) and carboxylic acid (0.48 mmol) were added and the resulting mixture was stirred at 40 °C for 4h. The crude material was subjected to column chromatography affording the corresponding compounds **43**–**56**.

2-(Allylamino)-2-oxoethyl octanoate (43). Yellow oil (94.1 mg, 0.39 mmol, 54 % yield). Eluent: PE/EtOAc 8:2. ^{1}H NMR (300 MHz, $CDCl_3$): $\delta = 6.33$ (br s, 1H), 5.77 (quint, $J = 5.8$ Hz, 1H), 5.18–5.08 (m, 2H), 4.51 (s, 2H), 3.86 (d, $J = 5.8$ Hz, 2H), 2.35 (t, $J = 9.5$ Hz, 2H), 1.60 (quint, $J = 9.5$ Hz, 2H), 1.26–1.22 (m, 8H), 0.83 (t, $J = 9.5$ Hz, 3H). ^{13}C NMR (75 MHz, $CDCl_3$): $\delta = 172.3$, 167.1, 133.7, 116.6, 62.9, 41.5, 34.0, 31.6, 29.0, 28.9, 24.8, 22.5, 14.0. IR (neat): $\tilde{\nu} = 3297$, 2925, 2360, 1746, 1664, 1539, 1423, 1260, 1022, 802 cm^{-1}. MS (ESI): *m/z* 242 $[M+H]^+$.

2-(Allylamino)-2-oxoethyl dodecanoate (44). White solid (107.1 mg, 0.36 mmol, 50 % yield). Eluent: PE/EtOAc 9:1. Mp 54.6–53.8 °C. ^{1}H NMR (300 MHz, $CDCl_3$): $\delta = 6.25$ (br s, 1H), 5.80 (quint, $J = 5.5$ Hz, 1H), 5.20–5.14 (m, 2H), 4.54 (s, 2H), 3.90 (d, $J = 5.5$ Hz, 2H), 2.37 (t, $J = 6.6$ Hz, 2H), 1.63 (t, $J = 6.6$ Hz, 2H), 1.26–1.18 (m, 16H), 0.85 (t, $J = 6.6$ Hz, 3H). ^{13}C NMR (75 MHz, $CDCl_3$): $\delta = 172.3$, 167.1, 133.8, 116.6, 62.9, 41.5, 34.0, 31.9, 29.6, 29.4, 29.3, 29.2, 29.1, 24.8, 24.5, 22.6, 14.0. IR (neat): $\tilde{\nu} = 3245$, 2921, 2361, 1736, 1663, 1540, 1418, 1238, 922, 776 cm^{-1}. MS (ESI): *m/z* 298 $[M+H]^+$.

(*R*,*Z*)-2-(Allylamino)-2-oxoethyl 12-(2-phenylacetoxy)octadec-9-enoate (45). Colorless oil (44.4 mg, 0.09 mmol, 18 % yield). Eluent: PE/EtOAc 9:1. ^{1}H NMR (300 MHz, $CDCl_3$): $\delta = 7.29$–7.26 (m, 5H), 6.18 (br s, 1H), 5.89–5.80 (m, 1H), 5.43 (q, $J = 6.3$ Hz, 1H), 5.28 (q, $J = 6.3$ Hz, 1H), 5.23–5.15 (m, 2H), 4.86 (quint, $J = 6.3$ Hz, 1H), 4.58 (s, 2H), 3.93 (t, $J = 5.5$ Hz, 2H), 3.58 (s, 2H), 2.40 (t, $J = 6.3$ Hz, 2H), 2.26 (q, $J = 6.3$ Hz, 2H), 1.97 (t, $J = 6.1$ Hz, 2H), 1.63 (q, $J = 6.3$ Hz, 2H), 1.50 (quint, $J = 6.1$ Hz, 2H), 1.29–1.20 (m, 16H), 0.85 (t, $J = 5.8$ Hz, 3H). ^{13}C NMR (75 MHz, $CDCl_3$): $\delta = 172.3$, 171.4, 167.1, 134.4, 133.7, 132.6, 129.3, 128.5, 127.0, 124.3, 116.9, 74.6, 63.0, 41.8, 41.5, 34.0, 33.6, 32.0, 31.7, 29.8, 29.6, 29.2, 29.1 (2C), 27.3, 25.3, 24.9, 22.6, 14.1. IR (neat): $\tilde{\nu} = 2926$, 2855, 1735, 1668, 1155, 722, 696 cm^{-1}. MS (ESI): *m/z* 536 $[M+Na]^+$. $[\alpha]_D^{20}$: +6.85 deg cm^3 g^{-1} dm^{-1} (*c* 0.012 g cm^{-3} in $CHCl_3$).

2-(Allylamino)-2-oxoethyl oleate (46). Colorless oil (132.9 mg, 0.35 mmol, 49 % yield). Eluent: PE/EtOAc 8:2. ^{1}H NMR (300 MHz, $CDCl_3$): $\delta = 6.29$ (br s, 1H), 5.79 (quint, $J = 5.8$ Hz, 1H), 5.31–5.29 (m, 2H), 5.18–5.18 (m, 2H), 4.54 (s, 2H), 3.88 (d, $J = 3.8$ Hz, 2H), 2.37 (t, $J = 5.5$ Hz, 2H), 1.98–1.94 (m, 4H), 1.62 (t, $J = 5.5$ Hz, 2H), 1.29–1.22 (m, 20H), 0.85 (t, $J = 5.5$ Hz, 3H). ^{13}C NMR (75 MHz, $CDCl_3$): $\delta = 172.3$, 167.0, 133.8, 130.1, 129.7, 116.7, 62.9, 41.5, 34.0, 31.9, 29.8, 29.7, 29.5, 29.3 (2C), 29.2, 29.1 (2C), 27.2 (2C), 24.8, 22.7, 14.1. IR (neat): $\tilde{\nu} = 3295$, 2923, 2360, 1748, 1664, 1539, 1460, 1161, 803, 722 cm^{-1}. MS (ESI): *m/z* 380 $[M+H]^+$.

(5*Z*,8*Z*,11*Z*,14*Z*)-2-(Allylamino)-2-oxoethyl icosa-5,8,11,14-tetraenoate (47). Yellow oil (132.5 mg, 0.33 mmol, 46 % yield). Eluent: PE/EtOAc 8:2.^{1}H NMR (300 MHz, $CDCl_3$): $\delta = 6.29$ (br s, 1H), 5.80 (quint, $J = 4.7$ Hz, 1H), 5.35–5.32 (m, 2H), 5.13 (d, $J = 4.7$ Hz, 2H), 3.89 (d, $J = 4.7$ Hz, 2H), 2.80–2.76 (m, 6H), 2.39 (t, $J = 3.6$ Hz, 2H), 2.12 (q, $J = 7.0$ Hz, 2H), 2.04 (q, $J = 7.0$ Hz, 2H), 1.75–1.71 (m, 2H), 1.38–1.17 (m, 6H), 0.87 (t, $J = 6.8$ Hz, 3H).^{13}C NMR (75 MHz, $CDCl_3$): $\delta = 172.1$, 167.0, 133.8, 130.5, 129.3, 128.6 (2C), 128.4, 128.0, 127.8, 127.6, 116.7, 63.0, 41.5, 33.3, 31.5, 29.3, 27.3, 26.5, 25.7 (3C), 24.7, 22.6, 14.0. IR (neat): $\tilde{\nu} = 3298$, 2925, 2326, 1747, 1664, 1540, 1425, 1147, 804, 708 cm^{-1}. MS (ESI): *m/z* 402 $[M+H]^+$.

(*E*)-2-(Allylamino)-2-oxoethyl 3,7-dimethylocta-2,6-dienoate (48). Whitish solid (63.6 mg, 0.24 mmol, 50 % yield). Eluent: PE/EtOAc 9:1. Mp 33–35 °C. ^{1}H NMR (300 MHz, $CDCl_3$): $\delta = 6.61$ (br s, 1H), 5.79–5.73 (m, 1H), 5.69 (s, 1H), 5.16–5.06 (m, 2H), 5.00 (t, $J = 6.2$ Hz, 1H), 4.54 (s, 2H), 3.87 (t, $J = 5.6$ Hz, 2H), 2.15–2.10 (m, 7H), 1.62 (s, 3H), 1.54 (s, 3H). ^{13}C NMR (75 MHz, $CDCl_3$): $\delta = 167.5$, 164.9, 163.4, 133.8, 132.7, 122.7, 116.6, 114.1, 62.2, 41.4, 41.1, 26.0, 25.7, 19.1, 17.7. IR (KBr): $\tilde{\nu} = 3286$, 3085, 2925, 1726, 1663, 1418, 1377, 1145, 921, 860 cm^{-1}. MS (ESI): *m/z* 266 $[M+H]^+$.

(4*E*,8*E*,12*E*,16*E*)-2-(Allylamino)-2-oxoethyl 4,8,13,17,21-pentamethyldocosa-4,8,12,16,20-pentaenoate (49). Colorless oil (154.3 mg, 0.31 mmol, 43 % yield). Eluent: PE/EtOAc 9:1. ^{1}H NMR (300 MHz, $CDCl_3$): $\delta = 6.15$ (br s, 1H), 5.85–5.79 (m, 1H), 5.17–5.11 (m, 7H), 4.60 (s, 2H), 3.93 (t, $J = 7.2$ Hz, 2H), 2.52 (t, $J = 7.7$ Hz, 2H), 2.33 (t, $J = 7.7$ Hz, 2H), 2.05–1.99 (m, 16H), 1.67–1.50 (m, 18H). ^{13}C NMR (75 MHz, $CDCl_3$): $\delta = 171.9$, 167.1, 135.2, 134.9, 134.8, 133.7, 133.0. 131.3, 125.6, 124.6, 124.5, 124.3 (2C), 116.8, 63.0, 41.5, 39.8 (2C), 39.6, 34.4, 33.0, 28.3 (2C), 26.8, 26.7 (2C), 25.8 (2C), 17.7, 16.1 (3C). IR (neat): $\tilde{\nu} = 3298$, 2918, 1748, 1665, 1438, 1380, 1149, 920, 849 cm^{-1}. MS (ESI): *m/z* 498 $[M+H]^+$.

2-(Cyclopropylamino)-2-oxoethyl octanoate (50). White solid (106.2 mg, 0.44 mmol, 91 % yield). Eluent: PE/EtOAc 7:3. Mp 81.3–82.8 °C. ^{1}H NMR (300 MHz, $CDCl_3$): $\delta = 6.40$ (br s, 1H), 4.44 (s, 2H), 2.65 (quint, $J = 3.0$ Hz, 1H), 2.31 (t, $J = 7.4$ Hz, 2H), 1.57 (quint, $J = 7.4$ Hz, 2H), 1.24–1.20 (m, 8H), 0.80 (t, $J = 6.3$ Hz, 3H), 0.71 (d, $J = 6.6$ Hz, 2H), 0.47 (d, $J = 6.6$ Hz, 2H). ^{13}C NMR (75 MHz, $CDCl_3$): $\delta = 172.3$, 168.5, 62.8, 33.9, 31.6, 29.0, 28.8, 24.8, 22.5, 22.3, 13.9, 6.4. IR (neat): $\tilde{\nu} = 3228$, 3073, 2917, 1744, 1656, 1566, 1167, 756, 583 cm^{-1}. MS (ESI): *m/z* 242 $[M+H]^+$.

2-(Cyclopropylamino)-2-oxoethyl dodecanoate (51). White solid (112.6 mg, 0.38 mmol, 79 % yield). Purified by crystallization with diethyl ether. Mp 90–91 °C. ^{1}H NMR (400 MHz, $CDCl_3$): $\delta = 6.18$ (br s, 1H), 4.52 (s, 2H), 2.74–2.72 (m, 1H), 2.38 (t, $J = 7.6$ Hz, 2H), 1.63 (quint, $J = 8.1$ Hz, 2H), 1.33–1.25 (m, 16H), 0.89–0.80 (m, 5H), 0.56–0.52 (m, 2H). ^{13}C NMR (101 MHz, $CDCl_3$): $\delta = 172.3$, 168.6, 63.0, 34.1, 32.0, 29.7 (2C), 29.5, 29.4, 29.2, 29.0, 24.9, 22.8, 22.3, 14.2, 6.7. IR (KBr): $\tilde{\nu} = 3225$, 3073, 2916, 2849, 1743, 1656, 1566, 1168, 758 cm^{-1}. MS (ESI): *m/z* 298 $[M+H]^+$.

(*R*,*Z*)-2-(Cyclopropylamino)-2-oxoethyl 12-(2-phenylacetoxy)octadec-9-enoate (52). Colorless oil (212.2 mg, 0.41 mmol, 86 % yield). Eluent: PE/EtOAc 8:2. ^{1}H NMR (300 MHz, $CDCl_3$): $\delta = 7.30$–7.24 (m, 5H), 6.16 (br s, 1H), 5.42 (q, $J = 7.1$ Hz, 1H), 5.27 (q, $J = 7.1$ Hz, 1H), 4.86 (quint, $J = 7.1$ Hz, 1H), 4.52 (s, 2H), 3.58 (s, 2H), 2.73 (sext, $J = 4.2$ Hz, 1H), 2.38 (t, $J = 7.1$ Hz, 2H), 2.2 (q, $J = 7.1$ Hz, 2H), 1.97 (t, $J = 6.3$ Hz, 2H), 1.64 (q, $J = 7.1$ Hz, 2H), 1.50 (quint, $J = 6.3$ Hz, 2H), 1.29–1.21 (m, 16H), 0.86–0.82 (m, 5H), 0.54–0.53 (m, 2H). ^{13}C NMR (75 MHz, $CDCl_3$): $\delta = 172.4$, 171.4, 168.7, 134.3, 132.6, 129.2, 128.5, 127.0, 124.2, 74.5, 62.7, 41.8, 33.9, 33.6, 32.0, 31.7, 29.7, 29.5, 29.2, 29.1 (2C), 27.3, 25.2, 24.8, 22.5, 22.3, 14.1, 6.4. IR (neat): $\tilde{\nu} = 2926$, 2854, 1733, 1669, 1530, 1155, 971, 899 cm^{-1}. MS (ESI): *m/z* 536 $[M+Na]^+$. $[\alpha]_D^{20}$: +17.42 deg cm^3 g^{-1} dm^{-1} (*c* 0.018 g cm^{-3} in $CHCl_3$).

2-(Cyclopropylamino)-2-oxoethyl oleate (53). White solid (159.4 mg, 0.42 mmol, 88 % yield). Eluent: PE/EtOAc 8:2. Mp 51.0–52.2 °C. ^{1}H NMR (300 MHz, $CDCl_3$): $\delta = 6.58$ (br s, 1H), 5.24 (q, $J = 5.1$ Hz, 2H), 4.42 (s, 2H), 2.63–2.61 (m, 1H), 2.30 (t, $J = 7.1$ Hz, 2H), 1.93–1.90 (m, 4H), 1.54 (quint, $J = 7.4$ Hz, 2H), 1.36–1.20 (m, 20H), 0.78 (t, $J = 6.7$ Hz, 3H), 0.68 (q, $J = 7.0$ Hz, 2H), 0.45–0.43 (m, 2H). ^{13}C NMR (75 MHz, $CDCl_3$): $\delta = 172.4$, 168.7, 130.0, 129.6, 62.7, 31.9, 29.8, 29.7, 29.5, 29.3 (2C), 29.2, 29.1 (2C), 27.2, 27.1, 24.8, 22.7, 22.3, 14.1, 6.4 (2C). IR (neat): $\tilde{\nu} = 3247$, 2920, 2851, 1744, 1677, 1560, 1171, 1003, 722, 581 cm^{-1}. MS (ESI): *m/z* 380 $[M+H]^+$.

2-(Cyclopropylamino)-2-oxoethyl (5Z,8Z,11Z,14Z)-icosa-5,8,11,14-tetraenoate (54). Yellow oil (172.7 mg, 0.43 mmol, 90 % yield). Eluent: PE/EtOAc 8:2. ^{1}H NMR (400 MHz, $CDCl_3$): $\delta = 6.23$ (br s, 1H), 5.43–5.28 (m, 8H), 4.50 (s, 2H), 2.83–2.77 (m, 6H), 2.74–2.68 (m, 1H), 2.39 (t, $J = 7.6$ Hz, 2H), 2.11 (q, $J = 7.2$ Hz, 2H), 2.03 (q, $J = 7.0$ Hz, 2H), 1.72 (quint, $J = 7.4$ Hz, 2H), 1.36–1.23 (m, 6H), 0.86 (t, $J = 6.7$ Hz, 3H), 0.81–0.76 (m, 2H), 0.54–0.50 (m, 2H). ^{13}C NMR (101 MHz, $CDCl_3$): $\delta = 172.1$, 168.5, 130.6, 129.3, 128.7, 128.6, 128.4, 128.1, 127.9, 127.6, 63.0, 33.3, 31.6, 29.4, 27.3, 26.5 (2C), 25.7 (2C), 24.6, 22.6, 22.3, 14.1, 6.6. IR (neat): $\tilde{\nu} = 3292$, 2928, 2857, 1744, 1666, 1537, 1265, 1148, 735 cm^{-1}. MS (ESI): *m/z* 402 $[M+H]^+$.

(*E*)-2-(Cyclopropylamino)-2-oxoethyl 3,7-dimethylocta-2,6-di

enoate (55). White solid (83.9 mg, 0.32 mmol, 66 % yield). Eluent: PE/EtOAC 8.5:1.5. Mp 81–83 °C. ^{1}H NMR (300 MHz, $CDCl_3$): $\delta = 6.31$ (br s, 1H), 5.69 (s, 1H), 5.03 (t, $J = 6.4$ Hz, 1H), 4.52 (s, 2H), 2.70 (sext, $J = 3.7$ Hz, 1H), 2.18–2.10 (m, 7H), 1.65 (s, 3H), 1.58 (s, 3H), 0.78–0.76 (m, 2H), 0.53–0.51 (m, 2H). ^{13}C NMR (75 MHz, $CDCl_3$): $\delta = 168.8$, 164.7, 163.1, 132.5, 122.5, 113.8, 62.0, 40.9, 25.8, 25.5, 22.0, 18.9, 17.5, 6.3. IR (KBr): $\tilde{\nu} = 3296$, 3071, 2918, 1723, 1665, 1457, 1386, 998, 825 cm^{-1}. MS (ESI): *m/z* 266 $[M+H]^+$.

(4*E*,8*E*,12*E*,16*E*)-2-(Cyclopropylamino)-2-oxoethyl 4,8,13,17,21-pentamethyldocosa-4,8,12,16,20-pentaenoate (56). Pale yellow oil (179.3 mg, 0.36 mmol, 75 % yield). Eluent: PE/EtOAc 9:1. ^{1}H NMR (300 MHz, $CDCl_3$): $\delta = 6.23$ (br s, 1H), 5.13–5.09 (m, 5H), 4.47 (s, 2H), 2.69 (sext, $J = 3.3$ Hz, 1H), 2.48 (t, $J = 7.8$ Hz, 2H), 2.30 (t, $J = 7.8$ Hz, 2H), 2.00–1.97 (m, 16H), 1.65–1.57 (m, 18H), 0.80–0.75 (m, 2H), 0.53–0.51 (m, 2H). ^{13}C NMR (75 MHz, $CDCl_3$): $\delta = 172.0$, 168.7, 135.0, 134.8, 134.6, 132.9, 131.7, 125.5, 124.6, 124.4, 124.3 (2C), 62.8, 39.7 (2C), 39.6, 34.4, 32.7, 28.3 (2C), 26.8 (2C), 26.6, 25.7 (2C), 22.1, 17.7, 16.0 (2C), 15.9, 6.4. IR (neat): $\tilde{\nu} = 3296$, 2917, 1747, 1664, 1444, 1381, 1150, 900, 843 cm^{-1}. MS (ESI): *m/z* 498 $[M+H]^+$.

4.2.3. General procedure for the synthesis of metabolites 57–59

As reported in Serafini et al. [61], the appropriate TBDMS-protected isocyanide **5**, **7** or **11** (0.90 mmol) was solubilized in CH_2Cl_2 (7 mL) and 37 % aqueous formaldehyde solution (99.82 μL, 3.6 mmol) and 2-(hydroxymethyl)benzoic acid (136.9 mg, 0.90 mmol) were added in order. The mixture was stirred at 40 °C overnight, then the volatile was removed under *vacuum* and ethyl acetate was added. The organic phase was washed with saturated aqueous solution of $NaHCO_3$ (x2), dried over sodium sulfate and evaporated. The crude material was solubilized in THF (5 mL) and cooled to 0 °C. At this temperature, acetic acid (113.3 μL, 1.98 mmol) and TBAF (1 M solution in THF, 1.98 mmol) were added. The reaction was stirred for 3h, then the volatile was evaporated and ethyl acetate was added, washed with water (x2), dried over sodium sulfate and evaporated. The crude material was subjected to column chromatography, affording compounds **57**–**59**.

***N*-(3,4-Dihydroxyphenethyl)-2-hydroxyacetamide (57).** Brown oil (73.9 mg, 0.35 mmol, 39 % yield). Eluent: PE/EtOAC 1:9. ^{1}H NMR (300 MHz, CD_3OD): $\delta = 6.70$ (d, $J = 6.7$ Hz, 1H), 6.67 (s, 1H), 6.54 (d, $J = 6.6$ Hz, 1H), 3.94 (s, 2H), 3.58–3.56 (m, 2H), 2.67–2.65 (m, 2H). ^{13}C NMR (75 MHz, $(CD3)_2CO$): $\delta = 172.1$, 145.1, 143.1, 130.9, 119.9, 115.8, 114.8, 61.7, 40.2, 35.0. IR (KBr): $\tilde{\nu} = 3291$, 2929, 1632, 1519, 1440, 1281, 1195, 1075, 783, 583 cm^{-1}. MS (ESI): *m/z* 212 $[M+H]^+$.

***N*-(4,5-Dihydroxy-2-iodophenethyl)-2-hydroxyacetamide (58).** Yellow solid (212.4 mg, 0.63 mmol, 70 % yield). Eluent: EtOAc/MeOH 9:1. Mp 150.4–151.0 °C. ^{1}H NMR (300 MHz, CD_3OD): $\delta = 7.21$ (s, 1H), 6.75 (s, 1H), 4.00 (s, 2H), 3.43–3.41 (m, 2H), 2.80–2.78 (m, 2H). ^{13}C NMR (75 MHz, CD_3OD) $\delta = 173.8$, 145.8, 144.9, 132.9, 125.5, 116.5, 86.0, 61.5, 39.3, 39.0. IR (KBr): $\tilde{\nu} = 3529$, 2926, 2343, 1734, 1654, 1506, 1068, 973, 875, 569 cm^{-1}. MS (ESI): *m/z* 360 $[M+Na]^+$.

2-Hydroxy-*N*-(2-hydroxyethyl)acetamide (59). Colorless oil (66.7 mg, 0.56 mmol, 62 % yield). Eluent: EtOAc/MeOH 9.5:0.5. ^{1}H NMR (300 MHz, $(CD_3)_2CO$): $\delta = 7.47$ (br s, 1H), 4.76 (br s, 1H), 4.12 (br s, 1H), 3.97 (s, 2H), 3.63 (t, $J = 5.7$ Hz, 2H), 3.38 (q, $J = 5.7$ Hz, 2H). ^{13}C NMR (75 MHz, $(CD_3)_2CO$): $\delta = 170.9$, 61.7, 60.9, 41.4. IR (neat): $\tilde{\nu} = 3272$, 3118, 1631, 1541, 1418, 1223, 1093, 1067, 761, 586 cm^{-1}. MS (ESI): *m/z* 120 $[M+H]^+$.

4.2.4. General procedure for the synthesis of compounds 60 and 61

The appropriate isocyanide **13** or **14** (0.90 mmol) was solubilized in CH_2Cl_2 (7 mL) and 37 % aqueous formaldehyde solution (99.82 μL, 3.6 mmol) and 2-(hydroxymethyl)benzoic acid (136.9 mg, 0.90 mmol) were added in order. The mixture was stirred at 40 °C overnight, then the volatile was removed under *vacuum* and ethyl acetate was added. The organic phase was washed with saturated aqueous solution of $NaHCO_3$ (x2), dried over sodium sulfate and evaporated. Purification by column chromatography afforded compounds **60** and **61**.

***N*-Allyl-2-hydroxyacetamide (60).** Colorless oil (69.1 mg, 0.60 mmol, 67 % yield). Eluent: PE/EtOAc 1:9. ^{1}H NMR (300 MHz, $CDCl_3$): $\delta = 6.67$ (br s, 1H), 5.84 (quint, $J = 6.0$ Hz, 1H), 5.23–5.13 (m, 2H), 4.11 (s, 2H), 3.93 (t, $J = 6.0$ Hz, 2H. ^{13}C NMR (75 MHz, $CDCl_3$): $\delta = 171.0$, 133.7, 116.7, 62.2, 41.4. IR (neat): $\tilde{\nu} = 3307$, 2921, 2852, 1639, 1542, 1457, 1261, 1075, 922, 566 cm^{-1}. MS (ESI): *m/z* 116 $[M+H]^+$.

***N*-Cyclopropyl-2-hydroxyacetamide (61).** Yellow solid (99.5 mg, 0.86 mmol, 96 % yield). Eluent: EtOAc. ^{1}H NMR (300 MHz, CD_3OD): $\delta = 3.96$ (s, 2H), 2.72–2.68 (m, 1H), 0.84–0.73 (m, 2H), 0.62–0.54 (m, 2H). ^{13}C NMR (75 MHz, CD_3OD): $\delta = 175.3$, 61.4, 21.8, 5.2. IR (neat): $\tilde{\nu} = 3276$, 1635, 1531, 1435, 1344, 1077, 820, 566 cm^{-1}. MS (ESI): *m/z* 116 $[M+H]^+$.

4.3. Biology

Assays for activity at human recombinant TRPV1 ion channel. HEK-293 cells stably expressing hTRPM8 or hTRPV1, were cultured in a monolayer in Earle's minimum essential medium with Earle's salts supplemented with 10 % fetal calf serum, 1 % nonessential amino acids, 2 mM L-glutamine, 100 μg streptomycin/mL, 100 U penicillin/mL, and 0.4 μg/mL puromycin (referred to as Puro-EMEM) and kept at 37 °C in a humidified atmosphere of 5 % CO_2 in a suitable incubator (STERI-CyCLE CO_2 Incubator Hepa Class 100, Thermo Electrón Corporation, Waltham, MA, USA). Cells were stored under liquid nitrogen and used for 15 generations from unfreezing. For fluorometric experiments, HEK-293 cells stably expressing hTRPV1 were detached by means of Trypsin/EDTA solution, resuspended in DMEM-10%FCS and seeded at a concentration of 4×10^4 cells/mL.

To measure the effectiveness of the compounds against TRPV1 activity we have used microfluorometry-based calcium flux assays with Fluo-4 NW Ca^{2+} dye and fluorescence as described previously [52]. Briefly human embryonic kidney (HEK) cell line stably transfected with hTRPV1 were seeded in 96-well plates at a cell density of 40.000 cells. After 2 days the medium was replaced with 100 μL of the dye loading solution Fluo-4 NW supplemented with probenecid 2.5 mM and incubated 1h at 37 °C. The TRP ion channel activity was measured using a POLASTAR plate reader (BMG Labtech, Ortenberg, Germany) setting the excitation wavelength at 485 nm and emission wavelength at 520 nm. The baseline fluorescence was recorded for 3 cycles before the addition of the vehicle, compound at different concentrations, and the antagonist (ruthenium red, 10 μM) (Fig. S1A, SI). DMSO, at the highest concentration used in the experiment, was added to the control wells. Fluorescence intensity was recorded during 7 more cycles and the agonist (capsaicin, 10 μM) was added. Fluorescence intensity was recorded during 10 more cycles. The maximum possible change detectable by the dye in the fluorescence assay was determined using 4 μM ionomycin in the assay (Fig. S7, SI).

Data analysis: The Z-factor was calculated in each assay using the following equation: (3 x (SDmax + SDmin))/(Mean max - Mean min). In all the experiments, the Z-factor was ≥0.5. The effect of the compounds against TRPV1 activity was determined by normalizing their effect to the maximum fluorescence observed with the application of 10 μM of capsaicin. A decrease in agonist signal was expressed as a percentage of inhibition (%). An increase in the fluorescence intensity at cycle 3 was expressed as a percentage of activation (%).

Data are expressed as the concentration exerting a half-maximal inhibition of agonist-induced (Ca^{2+})i elevation (IC_{50}, or concentration exerting a half-maximal activation of agonist-induced (Ca^{2+})i elevation (EC_{50}) which was calculated using GraphPad Prism® software (GraphPad Prism 7, Graphpad Software, San Diego, CA, USA) (Fig. S1B, SI). The equation used was Y = Bottom + (Top -Bottom)/(1 + 10((LogEC$_{50}$-X) x HillSlope)), with the restriction of the minimum (Bottom = 0). All determinations were performed in triplicate (n = 3) in 3 independent experiments (N = 3). All data are expressed as the mean ± standard deviation (SD).

Assays for activity at human recombinants cannabinoid CB1

and CB2 receptors. The HEK-CNG parental cell line, HEK-CNG-CB1 and HEK-CNG-CB2 cell lines were purchased from Codex BioSolutions, Inc. HEK-CNG cells were cultured in DMEM with 10 % FBS, 1 % P/S, and 25 mg/ml G418 at 37 °C and 5 % CO_2. HEK-CNG-CB1 and HEK-CNG-CB2 cells were cultured in DMEM with 10 % FBS, 1 % P/S, 25 mg/mL G418, and 5 mg/mL puromycin and kept at 37 °C in a humidified atmosphere of 5 % CO_2 in a suitable incubator (STERI-CyCLE CO_2 Incubator Hepa Class 100, Thermo Electrón Corporation, Waltham, MA, USA). Cells were passaged every 2–3 days or when confluence reached 80 %.

In order to determine functional pharmacology of the tested compound, HEK-CNG, HEK-CNG + CB1, and HEK-CNG + CB2 cells were plated at 70 000 cells/100 μL medium in clear poly-D-lysine coated 96 well plates in DMEM 10 % FBS, 1 % P/S medium the day before experiments were performed. Optimal confluence was 85 %, and above that CNG expression and CNBR expression declined.

The day of the experiment, ACTOne formulation Membrane Potential Dye was warmed to 37 °C and 100 μL added to each well, followed by 1 h incubation in the dark at room temperature. Plates were read using POLASTAR plate reader (BMG Labtech, Ortenberg, Germany) setting the excitation wavelength at 540 nm and emission wavelength at 590 nm.

The baseline fluorescence was recorded for 3 cycles before the addition of the tested compounds at different concentrations (from 1 M to 500 M) dissolved in 25 μM Ro 20–1724, and 800 nM forskolin in DPBS with 2.5 % (v/v) DMSO, agonist (100 nM CP-55,940) or antagonist (150 nM rimonabant to CB1 or 100 nM AM630 to CB2). After the addition of compounds, plates were read every 5 min for 60 min. The observed fluorescence signal increases as we activate cAMP production with forskolin and reaches steady state at 35 min, remaining constant up to 70 min. Taking into account the manufacturer's indications, analyses were done using the 50-min time point as recommended by the manufacturer (Fig. S2, SI). An acceptable run was defined as forskolin elevation of cAMP that was 2–3 times that of baseline (to ensure CNG expression), and CP-55,940 needed to suppress 70 % or more of the forskolin signal (to ensure CB1/CB2 expression) (Figs. S3A and S4A, SI. In addition, CP-55,940 EC_{50} needed to be around 50 nM for CB1 or 17 nM for CB2 (Figs. S3B,C and S4B,C, SI). Specificity was established by comparison with HEK-CNG cells. Anandamide, included as a control (Fig. S5, SI), displayed a potency in agreement with data reported in the literature [64]. At least six biological replicates were used for subsequent data analysis. Data analysis was done in GraphPad Prism 6.0 with non-linear analysis.

All determinations were performed in triplicate (n = 3) in 3 independent experiments (N = 3). All data are expressed as the mean ± standard deviation (SD).

Patch clamp assays. Patch-clamp recordings were conducted on HEK293-hTRPV1 cells seeded on 12 mmØ glass coverslips treated with poly-L-lysine solution (Sigma Aldrich, Spain) two days prior the experiments [65]. The internal pipette solution consisted of (in mM) 150 NaCl, 5 EGTA, 3 $MgCl_2$, and 10 HEPES, adjusted to pH 7.2 with CsOH. The extracellular solution contained (in mM) 150 NaCl, 6 CsCl, 1.5 $CaCl_2$, 1 $MgCl_2$, 10 D-glucose, and 10 HEPES, adjusted to pH 7.4 with NaOH. In the case of dose-response assays the Ca^{2+} concentration of the extracellular solution was reduced to 0.1 mM to minimize the impact of receptor desensitization on the EC_{50} value.

The patch pipettes used in the experiment were created from thin-wall borosilicate capillary glass tubing and were pulled to a final resistance of 2–8 MΩ when filled with the internal solution. The pulling process was carried out using a horizontal flaming/brown Micropipette puller Model P-97 from Sutter Instrument. Recordings were obtained at a sampling rate of 10 kHz and subsequently low-pass filtered at 3 kHz. Any recordings that showed leak currents greater than 200 pA or series resistance exceeding 20 MΩ were excluded from the analysis.

During voltage-clamp recordings, the cells were held at a constant potential, and various modulators were applied as part of the experimental protocol (Fig. S6, SI). To ensure consistency in data analysis, total currents were normalized to the first current peak evoked by a stimulus. TRPV1 activity was assessed by applying two pulses of 0.5 μM Capsaicin with a 2-min interval or two pulses of the compound **41**. The application of capsaicin or **41**, directly onto the investigated cell, was achieved through a multibarrel concentration-clamp device coupled to electronically driven miniature solenoid valves controlled by PatchMaster software (HEKA Electronics, Lambrecht, Germany).

Data were sampled at 10 kHz using an EPC10 amplifier with PatchMaster 2.53 software (HEKA Electronics, Lambrecht, Germany). The analysis was performed with PatchMaster 2.53 and GraphPad Prism 8.0 (Graphpad Software, San Diego, CA, USA). All measurements were conducted at 24–26 °C. Whole-cell patch-clamp experiments were analysed as the percentage of activation of the TRPV1 channel. This was achieved by normalizing the ratio (p2/p1) of testing conditions to the ratio (p2/p1) of the control condition. GraphPad 8.0 was used for data analysis, a non-linear regression curve and EC_{50} were obtained by plotting log (agonist) vs. response fitting the curve to Hill equation:

$$Y=Bottom + (X^{\wedge}HillSlope)*(Top-Bottom)/(X^{\wedge}HillSlope + EC_{50}{}^{\wedge}HillSlope)$$

All data were expressed as the mean ± standard error of the mean (SEM) (N = 3; n = 6–8).

Cell cultures for skin homogenate. HaCaT cells were grown in Dulbecco's Modified Eagle's Medium (DMEM) (Sigma-Aldrich, St. Louis, MO) supplemented with 10 % fetal bovine serum (FBS, Gibco, Italy), 2 mM glutamine (Sigma-Aldrich, St. Louis, MO), 10 units/mL penicillin, and 100 g/mL streptomycin (Sigma-Aldrich, St. Louis, MO).

Primary adult epidermal keratinocytes were purchased from American Type Culture Collection (ATCC, Manassas, VA, USA) (ATCC®, PCS 200-011™) and maintained as reported in Serafini et al., 2018 [52]. Briefly, cells were cultured in Dermal Cell Basal Media (ATCC, PCS 200−030) supplemented with Keratinocyte Growth kit components (Bovine Pituitary Extract (BPE), recombinant tumor growth factor alpha (rhTGFα), L-glutamine, hydrocortisone hemi-succinate, insulin, epinephrine, and apotransferrin, (ATCC PCS 200-040), 10 units/mL penicillin and 100 μg/mL streptomycin (Sigma-Aldrich, St. Louis, MO)). Primary adult dermal fibroblasts were purchased from American Type Culture Collection (ATCC, Manassas, VA, USA) (ATCC®, PCS 200-012™) and maintained as reported in Serafini et al., 2018 [52]. Briefly, cells were cultured in Fibroblast Media supplemented with fibroblast growth kit-low serum, containing L-glutamine, hydrocortisone, hemi-succinate, recombinant fibroblast growth factor beta (rhFGFβ), rh-insulin, ascorbic acid, and FBS, (ATCC PCS-201- 041), 10 units/mL penicillin, and 100 μg/mL streptomycin (Sigma-Aldrich, St. Louis, MO).

All the cell lines were maintained at 37 °C in a humidified incubator with 5 % CO_2/95 % air and subcultured as needed by detaching the cells with 0.25 % trypsin and 5 mM EDTA. As described in Serafini et al. [52], 2018, 10^7 cells were lysed in a pH 7.5 Tris-HCl buffer (20 mM) (supplemented with proteases inhibitors cocktail, Sigma-Aldrich, St. Louis, MO). Trypan blue staining was used to detect the lack of intact cells. The samples were centrifuged for 10 min at 12000 g at 4 °C, and the supernatants were collected and measured using Bradford (Bio-rad, Hercules, United States).

Metabolic stability. (a) Human recovered plasma pooled (088SER-PLP-K3EDTA) was purchased from Tebu-bio (Magenta, Italy). The incubation (70 μL final volume) was carried out at the final concentration of 50 μM by dissolving each tested compound in DMSO (5 % final volume) in preincubated plasma at 37 °C. The mixture was shaken for 60 min at 37 °C. Control incubations were carried out without the substrate. Each incubation was performed in triplicate and stopped by addition of 140 μL of ice-cold acetonitrile, vortexed, and centrifuged at 13000 r.p.m. for 10 min before analysis. (b) Human skin and liver S9 fraction, (pooled mixed sex, 20 individual donors, protein concentration: 20 mg/mL)

were purchased from Corning B.V. Life Sciences (Amsterdam, The Netherlands). The incubation mixture (150 μL final volume) was carried out in a 50 mM TRIS (Tris[hydroxymethyl]aminomethane) buffer (pH 7.4) containing tween 80 surfactant (2.5 mg/mL), and substrate compounds at the 5 μM final concentration. After pre-equilibration of the mixture, an appropriate volume of S9 suspension was added to give a final protein concentration of 1.0 mg/mL. The mixture was shaken for 60 min at 37 °C. Control incubations were carried out without S9 fractions. Each incubation was performed in triplicate and was stopped by addition of 150 μL ice-cold acetonitrile, vortexed, and centrifuged at 13000 r.p.m. for 10 min before analysis. (c) The standard incubation mixture (100 μL final volume) was carried out in a 50 mM TRIS (Tris [hydroxymethyl]aminomethane) buffer (pH 7.4) containing tween 80 surfactant (2.5 mg/mL) substrate compounds at the 5 μM final concentration. After pre-equilibration of the mixture, an appropriate volume of HaCaT, epidermal keratinocytes and dermal fibroblasts homogenates were added to give a final protein concentration of 40 μg/mL. Samples were shaken for 120 min at 37 °C. Control incubations were carried out without homogenates. Each incubation was performed in triplicate and stopped by addition of 100 μL of ice-cold acetonitrile, vortexed and centrifuged at 13000 r.p.m. for 10 min before analysis.

4.4. Molecular modeling and docking

Human TRPV1 was modelled using the structure of the squirrel TRPV1 in complex with capsaicin (PDB ID: 7LR0) [62] determined by electron microscopy at 3.81 Å resolution. Human CB2 was modelled using the structure of CB2 in complex with the agonist AM12033 (PDB ID: 6KPF) [63], determined by electron microscopy at 2.90 Å resolution; both protein structures were used to explore binding modes of compound **41**.

The docking procedure was performed with Autodock4 algorithm [66] implemented in Yasara [67,68]. Briefly, a local docking procedure was accomplished using either human TRPV1 model or human CB2 structure, and compound **41**. The search space was limited to a simulation box built 5 Å around the well-known agonist ligands (capsaicin and AM12033 for TRPV1 and CB2, respectively). A total of 500 flexible docking runs were set and clustered around the selected binding sites. The program performs a simulated annealing minimization of the complexes, which moves the structure to a stable energy minimum, by using the implemented AMBER 99 (Assisted Model Building with Energy Refinement) force field [69]. The Yasara pH command was set to 7.0, to ensure that molecules preserved their pH dependency of bond orders and protonation patterns. The best binding energy complex in each cluster was stored, analysed, and used to select the best orientation of the interacting partners. The theoretical affinities of ligands at its binding site were determined by calculating the binding energy of the ligand-receptor complex. The binding energy was obtained by measuring the energy at infinite distance (the unbound state) and subtracting from that value the energy of the complex at the bound state. Figures were drawn using the open source PyMol v2.6 (The PyMOL Molecular Graphics System, Version 1.8 Schrödinger, LLC, at http://www.pymol.org/). Interactions were determined in PLIP (https://plip-tool.biotec.tu-dresden.de/plip-web/plip/index), a fully automated web server [70] to identify non-covalent interactions between macromolecules and ligands.

CRediT authorship contribution statement

Angela Lamberti: Validation, Methodology, Data curation. **Marta Serafini:** Methodology, Data curation. **Silvio Aprile:** Methodology, Formal analysis, Data curation. **Irene Preet Bhela:** Methodology, Data curation. **Georgia Goutsiou:** Methodology, Data curation. **Emanuela Pessolano:** Methodology, Data curation. **Gregorio Fernandez-Ballester:** Methodology, Data curation. **Antonio Ferrer-Montiel:** Writing – review & editing, Supervision, Data curation, Conceptualization. **Rita Maria Concetta Di Martino:** Writing – review & editing, Writing – original draft, Supervision, Data curation. **Asia Fernandez-Carvajal:** Writing – review & editing, Writing – original draft, Supervision, Data curation, Conceptualization. **Tracey Pirali:** Writing – review & editing, Writing – original draft, Supervision, Data curation, Conceptualization.

Declaration of competing interest

The authors declare that they have no known competing financial interests or personal relationships that could have appeared to influence the work reported in this paper.

Data availability

No data was used for the research described in the article.

Acknowledgements

This work is part of the project NODES which has received funding from the MUR–M4C2 1.5 of PNRR with grant agreement no. ECS00000036 (to R.M.C.D.M. and T.P.), AIRC under IG 2023 - ID. 29452 project (to T.P.), the Agencia Estatal de Investigación grant no. PID2021-12643OB-C21 and the Generalitat Valenciana project PROMETEO/2021/031 (to A.F.-C and A.F.-M) co-funded with FEDER funds from EU "Una manera de hacer Europa. G.G. and A.L. are supported by the European Union's Horizon 2020 Research and Innovation Program under the Marie Skłodowska-Curie Actions grant agreement no. 956477 (PIANO). Graphical abstract was edited with BioRender.

Appendix A. Supplementary data

Supplementary data to this article can be found online at https://doi.org/10.1016/j.ejmech.2024.116845.

Abbreviations used

2-AG	2-arachidonoylglicerol
AEA	anandamide
AMBER	assisted model building with energy refinement
BPE	bovine pituitary extract
CBG	cannabigerol
CNG	cyclic nucleotide gated channel
Cryo-EM	cryogenic-electron microscopy
DPBS	Dulbecco's phosphate-buffered saline
EC	endocannabinoid
EMEM	Earle's minimum essential medium

(*continued on next page*)

(*continued*)

Et_2O	diethyl ether
EtOAc	ethyl acetate
EV	endovanilloid
FBS	fetal bovine serum
HaCaT	immortalized nontumorigenic human epidermal
NADA	*N*-arachidonoyl-dopamine
OLDA	*N*-oleoyl-dopamine
PE	petroleum ether
TBDMS	*tert*-butyldimethylsilyl
TEBA	benzyltriethylammonium chloride
TGFα	tumor growth factor alpha
THC	delta-9-tetrahydrocannabidiol
TRP	transient receptor potential
TRPA1	transient receptor potential cation channel subfamily A member 1
TRPM8	transient receptor potential cation channel subfamily M member 8
TRPV1	thermosensory channel TRP vanilloid 1

References

[1] A.-P. Koivisto, M.G. Belvisi, R. Gaudet, A. Szallasi, Advances in TRP channel drug discovery: from target validation to clinical studies, Nat. Rev. Drug Discov. 21 (1) (2022) 41–59, https://doi.org/10.1038/s41573-021-00268-4.

[2] S.J. Conway, TRPing the switch on pain: an introduction to the chemistry and biology of capsaicin and TRPV1, Chem. Soc. Rev. 37 (8) (2008) 1530–1545, https://doi.org/10.1039/B610226N.

[3] D.D. McKemy, W.M. Neuhausser, D. Julius, Identification of a cold receptor reveals a general role for TRP channels in thermosensation, Nature 416 (6876) (2002) 52–58, https://doi.org/10.1038/nature719.

[4] T. Xiao, M. Sun, C. Zhao, J. Kang, TRPV1: a promising therapeutic target for skin aging and inflammatory skin diseases, Front. Pharmacol. 14 (2023) 1037925, https://doi.org/10.3389/fphar.2023.1037925.

[5] V.Y. Moiseenkova-Bell, L.A. Stanciu, I.I. Serysheva, B.J. Tobe, T.G. Wensel, Structure of TRPV1 channel revealed by electron cryomicroscopy, Proc. Natl. Acad. Sci. U. S. A. 105 (21) (2008) 7451–7455, https://doi.org/10.1073/pnas.0711835105.

[6] E. Cao, M. Liao, Y. Cheng, D. Julius, TRPV1 structures in distinct conformations reveal activation mechanisms, Nature 504 (7478) (2013) 113–118, https://doi.org/10.1038/nature12823.

[7] A. Neuberger, M. Oda, Y.A. Nikolaev, K.D. Nadezhdin, E.O. Gracheva, S. N. Bagriantsev, A.I. Sobolevsky, Human TRPV1 structure and inhibition by the analgesic SB-366791, Nat. Commun. 14 (1) (2023) 2451, https://doi.org/10.1038/s41467-023-38162-9.

[8] D. Bustos, C. Galarza, W. Ordoñez, S. Brauchi, B. Benso, Cost-effective Pipeline for a rational design and selection of capsaicin analogues targeting TRPV1 channels, ACS Omega 8 (13) (2023) 11736–11749, https://doi.org/10.1021/acsomega.2c05672.

[9] S.E. Thomas, H. Laycock, The use of high dose topical capsaicin in the management of peripheral neuropathy: narrative review and local experience, Br. J. Pain 14 (2) (2020) 133–140, https://doi.org/10.1177/2049463720914332.

[10] J. Ann, H.S. Kim, S.A. Thorat, H. Kim, H.J. Ha, K. Choi, Y.H. Kim, M. Kim, S. W. Hwang, L.V. Pearce, T.E. Esch, N.A. Turcios, P.M. Blumberg, J. Lee, Discovery of Nonpungent transient receptor potential vanilloid 1 (TRPV1) agonist as Strong topical analgesic, J. Med. Chem. 63 (1) (2020) 418–424, https://doi.org/10.1021/acs.jmedchem.9b01046.

[11] A. Szallasi, D.N. Cortright, C.A. Blum, S.R. Eid, The vanilloid receptor TRPV1: 10 years from channel cloning to antagonist proof-of-concept, Nat. Rev. Drug Discov. 6 (5) (2007) 357–372, https://doi.org/10.1038/nrd2280.

[12] A. Fernández-Carvajal, R. González-Muñiz, G. Fernández-Ballester, A. Ferrer-Montiel, Investigational drugs in early phase clinical trials targeting thermotransient receptor potential (thermoTRP) channels, Expert Opin. Investig. Drugs 29 (11) (2020) 1209–1222, https://doi.org/10.1080/13543784.2020.1825680.

[13] C.W. Park, B.J. Kim, Y.W. Lee, C. Won, C.O. Park, B.Y. Chung, D.H. Lee, K. Jung, H. J. Nam, G. Choi, Y.H. Park, K.H. Kim, M. Park, Asivatrep, a TRPV1 antagonist, for the topical treatment of atopic dermatitis: phase 3, randomized, vehicle-controlled study (CAPTAIN-AD), J. Allergy Clin. Immunol. 149 (4) (2022) 1340–1347.e4, https://doi.org/10.1016/j.jaci.2021.09.024.

[14] C.J. Fowler, The endocannabinoid system - current implications for drug development, J. Intern. Med. 290 (1) (2021) 2–26, https://doi.org/10.1016/j.jaci.2021.09.024.

[15] V.D. Marzo, M. Bifulco, L.D. Petrocellis, The endocannabinoid system and its therapeutic exploitation, Nat. Rev. Drug Discov. 3 (9) (2004) 771–784, https://doi.org/10.1038/nrd1495.

[16] R.M.P. Campos, A.F.L. Aguiar, Y. Paes-Colli, P.M.P. Trindade, B.K. Ferreira, R.A. de Melo Reis, L.S. Sampaio, Cannabinoid therapeutics in chronic neuropathic pain: from animal research to human treatment, Front. Physiol. 12 (2021) 785176, https://doi.org/10.3389/fphys.2021.785176.

[17] N. Clayton, F.H. Marshall, C. Bountra, C.T. O'Shaughnessy, CB1 and CB2 cannabinoid receptors are implicated in inflammatory pain, Pain 96 (3) (2002) 253–260, https://doi.org/10.1016/S0304-3959(01)00454-7.

[18] C.D. Río, E. Millán, V. García, G. Appendino, J. DeMesa, E. Muñoz, The endocannabinoid system of the skin. A potential approach for the treatment of skin disorders, Biochem. Pharmacol. 157 (2018) 122–133, https://doi.org/10.1016/j.bcp.2018.08.022.

[19] T. Hua, K. Vemuri, M. Pu, L. Qu, G.W. Han, Y. Wu, S. Zhao, W. Shui, S. Li, A. Korde, R.B. Laprairie, E.L. Stahl, J.H. Ho, N. Zvonok, H. Zhou, I. Kufareva, B. Wu, Q. Zhao, M.A. Hanson, L.M. Bohn, A. Makriyannis, R.C. Stevens, Z.J. Liu, Crystal structure of the human cannabinoid receptor CB(1), Cell 167 (3) (2016) 750–762.e14, https://doi.org/10.1016/j.cell.2016.10.004.

[20] X. Li, T. Hua, K. Vemuri, J.H. Ho, Y. Wu, L. Wu, P. Popov, O. Benchama, N. Zvonok, K. Locke, L. Qu, G.W. Han, M.R. Iyer, R. Cinar, N.J. Coffey, J. Wang, M. Wu, V. Katritch, S. Zhao, G. Kunos, L.M. Bohn, A. Makriyannis, R.C. Stevens, Z.J. Liu, Crystal structure of the human cannabinoid receptor CB2, Cell 176 (3) (2019) 459–467.e13, https://doi.org/10.1016/j.cell.2018.12.011.

[21] M. Soethoudt, U. Grether, J. Fingerle, T.W. Grim, F. Fezza, L. de Petrocellis, C. Ullmer, B. Rothenhäusler, C. Perret, N. van Gils, D. Finlay, C. MacDonald, A. Chicca, M.D. Gens, J. Stuart, H. de Vries, N. Mastrangelo, L. Xia, G. Alachouzos, M.P. Baggelaar, A. Martella, E.D. Mock, H. Deng, L.H. Heitman, M. Connor, V. Di Marzo, J. Gertsch, A.H. Lichtman, M. Maccarrone, P. Pacher, M. Glass, M. van der Stelt, Cannabinoid CB(2) receptor ligand profiling reveals biased signalling and off-target activity, Nat. Commun. 8 (2017) 13958, https://doi.org/10.1038/ncomms13958.

[22] Z.M. Whiting, J. Yin, S.M. de la Harpe, A.J. Vernall, N.L. Grimsey, Developing the Cannabinoid receptor 2 (CB2) pharmacopoeia: past, present, and future, Trends Pharmacol. Sci. 43 (9) (2022) 754–771, https://doi.org/10.1016/j.tips.2022.06.010.

[23] R. Smoum, U. Grether, M. Karsak, A.J. Vernall, F. Park, C.J. Hillard, P. Pacher, Editorial: therapeutic potential of the cannabinoid CB2 receptor, Front. Pharmacol. 13 (2022) 1039564, https://doi.org/10.3389/fphar.2022.1039564.

[24] L. Cristino, L. de Petrocellis, G. Pryce, D. Baker, V. Guglielmotti, V. Di Marzo, Immunohistochemical localization of cannabinoid type 1 and vanilloid transient receptor potential vanilloid type 1 receptors in the mouse brain, Neuroscience 139 (4) (2006) 1405–1415, https://doi.org/10.1016/j.neuroscience.2006.02.074.

[25] U. Anand, W.R. Otto, D. Sanchez-Herrera, P. Facer, Y. Yiangou, Y. Korchev, R. Birch, C. Benham, C. Bountra, I.P. Chessell, P. Anand, Cannabinoid receptor CB2 localisation and agonist-mediated inhibition of capsaicin responses in human sensory neurons, Pain 138 (3) (2008) 667–680, https://doi.org/10.1016/j.pain.2008.06.007.

[26] F. Rossi, D. Siniscalco, L. Luongo, L. De Petrocellis, G. Bellini, S. Petrosino, M. Torella, C. Santoro, B. Nobili, S. Perrotta, V. Di Marzo, S. Maione, The endovanilloid/endocannabinoid system in human osteoclasts: possible involvement in bone formation and resorption, Bone 44 (3) (2009) 476–484, https://doi.org/10.1016/j.bone.2008.10.056.

[27] Y. Li, X. Chen, Y. Nie, Y. Tian, X. Xiao, F. Yang, Endocannabinoid activation of the TRPV1 ion channel is distinct from activation by capsaicin, J. Biol. Chem. 297 (3) (2021) 101022, https://doi.org/10.1016/j.jbc.2021.101022.

[28] V. Di Marzo, F. Piscitelli, The endocannabinoid system and its modulation by phytocannabinoids, Neurotherapeutics 12 (4) (2015) 692–698, https://doi.org/10.1007/s13311-015-0374-6.

[29] W.R. Arnold, L.N. Carnevale, Z. Xie, J.L. Baylon, E. Tajkhorshid, H. Hu, A. Das, Anti-inflammatory dopamine- and serotonin-based endocannabinoid epoxides reciprocally regulate cannabinoid receptors and the TRPV1 channel, Nat. Commun. 12 (1) (2021) 926, https://doi.org/10.1038/s41467-021-20946-6.

[30] N. Malek, K. Starowicz, Dual-acting compounds targeting endocannabinoid and endovanilloid systems-a novel treatment option for chronic pain management, Front. Pharmacol. 7 (2016) 257, https://doi.org/10.3389/fphar.2016.00257.

[31] R. Wi, Y.C. Chung, B.K. Jin, Functional crosstalk between CB and TRPV1 receptors protects nigrostriatal dopaminergic neurons in the MPTP model of Parkinson's

disease, J. Immunol. Res. 2020 (2020) 5093493, https://doi.org/10.1155/2020/5093493.
[32] T. Bíró, B.I. Tóth, G. Haskó, R. Paus, P. Pacher, The endocannabinoid system of the skin in health and disease: novel perspectives and therapeutic opportunities, Trends Pharmacol. Sci. 30 (8) (2009) 411–420, https://doi.org/10.1016/j.tips.2009.05.004.
[33] M.J. Caterina, TRP channel cannabinoid receptors in skin sensation, homeostasis, and inflammation, ACS Chem. Neurosci. 5 (11) (2014) 1107–1116, https://doi.org/10.1021/cn5000919.
[34] C. Muller, P. Morales, P.H. Reggio, Cannabinoid ligands targeting TRP channels, Front. Mol. Neurosci. 11 (2018) 487, https://doi.org/10.3389/fnmol.2018.00487.
[35] C. Muller, D.L. Lynch, D.P. Hurst, P.H. Reggio, A Closer look at anandamide interaction with TRPV1, Front. Mol. Biosci. 7 (2020) 144, https://doi.org/10.3389/fmolb.2020.00144.
[36] S.M. Huang, T. Bisogno, M. Trevisani, A. Al-Hayani, L. De Petrocellis, F. Fezza, M. Tognetto, T.J. Petros, J.F. Krey, C.J. Chu, J.D. Miller, S.N. Davies, P. Geppetti, J. M. Walker, V. Di Marzo, An endogenous capsaicin-like substance with high potency at recombinant and native vanilloid VR1 receptors, Proc. Nat. Acad. Sci. U. S. A. 99 (12) (2002) 8400–8405, https://doi.org/10.1073/pnas.122196999.
[37] C.J. Chu, S.M. Huang, L. De Petrocellis, T. Bisogno, S.A. Ewing, J.D. Miller, R. E. Zipkin, N. Daddario, G. Appendino, V. Di Marzo, J.M. Walker, N-oleoyldopamine, a novel endogenous capsaicin-like lipid that produces hyperalgesia, J. Biol. Chem. 278 (16) (2003) 13633–13639, https://doi.org/10.1074/jbc.M211231200.
[38] T. Sugiura, S. Kondo, A. Sukagawa, S. Nakane, A. Shinoda, K. Itoh, A. Yamashita, K. Waku, 2-Arachidonoylglycerol: a possible endogenous cannabinoid receptor ligand in brain, Biochem. Biophys. Res. Commun. 215 (1) (1995) 89–97, https://doi.org/10.1006/bbrc.1995.2437.
[39] G. Appendino, A. Ligresti, A. Minassi, M.G. Cascio, M. Allarà, O. Taglialatela-Scafati, R.G. Pertwee, L. De Petrocellis, V. Di Marzo, Conformationally constrained fatty acid ethanolamides as cannabinoid and vanilloid receptor probes, J. Med. Chem. 52 (9) (2009) 3001–3009, https://doi.org/10.1021/jm900130m.
[40] V. Di Marzo, T. Bisogno, L. De Petrocellis, I. Brandi, R.G. Jefferson, R.L. Winckler, J.B. Davis, O. Dasse, A. Mahadevan, R.K. Razdan, B.R. Martin, Highly selective CB (1) cannabinoid receptor ligands and novel CB(1)/VR(1) vanilloid receptor "hybrid" ligands, Biochem. Biophys. Res. Commun. 281 (2) (2001) 444–451, https://doi.org/10.1006/bbrc.2001.4354.
[41] E. de Lago, P. Urbani, J.A. Ramos, V. Di Marzo, J. Fernández-Ruiz, Arvanil, a hybrid endocannabinoid and vanilloid compound, behaves as an antihyperkinetic agent in a rat model of Huntington's disease, Brain Res. 1050 (1–2) (2005) 210–216, https://doi.org/10.1016/j.brainres.2005.05.024.
[42] M. Tham, O. Yilmaz, M. Alaverdashvili, M.E.M. Kelly, E.M. Denovan-Wright, R. B. Laprairie, Allosteric and orthosteric pharmacology of cannabidiol and cannabidiol-dimethylheptyl at the type 1 and type 2 cannabinoid receptors, Br. J. Pharmacol. 176 (10) (2019) 1455–1469, https://doi.org/10.1111/bph.14440.
[43] G. Appendino, M.G. Cascio, S. Bacchiega, A.S. Moriello, A. Minassi, A. Thomas, R. Ross, R. Pertwee, L. De Petrocellis, V. Di Marzo, First "hybrid" ligands of vanilloid TRPV1 and cannabinoid CB2 receptors and non-polyunsaturated fatty acid-derived CB2-selective ligands, FEBS Lett. 580 (2) (2006) 568–574, https://doi.org/10.1016/j.febslet.2005.12.069.
[44] V. Di Marzo, New approaches and challenges to targeting the endocannabinoid system, Nat. Rev. Drug Discov. 17 (9) (2018) 623–639, https://doi.org/10.1038/nrd.2018.115.
[45] A.L. Hopkins, Network pharmacology: the next paradigm in drug discovery, Nat. Chem. Biol. 4 (11) (2008) 682–690, https://doi.org/10.1038/nchembio.118.
[46] G.F. Mangiatordi, F. Intranuovo, P. Delre, F.S. Abatematteo, C. Abate, M. Niso, T. M. Creanza, N. Ancona, A. Stefanachi, M. Contino, Cannabinoid receptor subtype 2 (CB2R) in a multitarget approach: perspective of an innovative strategy in cancer and neurodegeneration, J. Med. Chem. 63 (23) (2020) 14448–14469, https://doi.org/10.1021/acs.jmedchem.0c01357.
[47] A. Angeli, L. Micheli, F. Carta, M. Ferraroni, T. Pirali, A. Fernandez Carvajal, A. Ferrer Montiel, L. Di Cesare Mannelli, C. Ghelardini, C.T. Supuran, First-in-class dual hybrid carbonic anhydrase inhibitors and transient receptor potential vanilloid 1 agonists revert oxaliplatin-induced neuropathy, J. Med. Chem. 66 (2) (2023) 1616–1633, https://doi.org/10.1021/acs.jmedchem.2c01911.
[48] F. Intranuovo, L. Brunetti, P. DelRe, G.F. Mangiatordi, A. Stefanachi, A. Laghezza, M. Niso, F. Leonetti, F. Loiodice, A. Ligresti, M. Kostrzewa, J. Brea, M.I. Loza, E. Sotelo, M. Saviano, N.A. Colabufo, C. Riganti, C. Abate, M. Contino, Development of *N*-(1-adamantyl)benzamides as novel anti-inflammatory multitarget agents acting as dual modulators of the cannabinoid CB2 receptor and fatty acid amide hydrolase, J. Med. Chem. 66 (1) (2023) 235–250, https://doi.org/10.1021/acs.jmedchem.2c01084.
[49] P. Morales, C. Muller, N. Jagerovic, P.H. Reggio, Targeting CB2 and TRPV1: computational approaches for the identification of dual modulators, Front. Mol. Biosci. 9 (2022), https://doi.org/10.3389/fmolb.2022.841190, 841190. 841190.
[50] M.J. Buskes, A. Coffin, D.M. Troast, R. Stein, M.-J. Blanco, Accelerating drug discovery: synthesis of complex chemotypes via multicomponent reactions, ACS Med. Chem. Lett. 14 (4) (2023) 376–385, https://doi.org/10.1021/acsmedchemlett.3c00012.
[51] M. Passerini, L. Simone, Sopra gli isonitrili (I). Composto del *p*-isonitril-azobenzolo con acetone ed acido acetico, Gazz. Chim. Ital. 51 (1921) 126–129.
[52] M. Serafini, A. Griglio, S. Aprile, F. Seiti, C. Travelli, F. Pattarino, G. Grosa, G. Sorba, A.A. Genazzani, S. Gonzalez-Rodriguez, L. Butron, I. Devesa, A. Fernandez-Carvajal, T. Pirali, A. Ferrer-Montiel, Targeting transient receptor potential vanilloid 1 (TRPV1) channel softly: the discovery of Passerini adducts as a topical treatment for inflammatory skin disorders, J. Med. Chem. 61 (10) (2018) 4436–4455, https://doi.org/10.1021/acs.jmedchem.8b00109.
[53] A. Fernández-Carvajal, G. Fernández-Ballester, A. Ferrer-Montiel, TRPV1 in chronic pruritus and pain: soft modulation as a therapeutic strategy, Front. Mol. Neurosci. 15 (2022) 930964, https://doi.org/10.3389/fnmol.2022.930964.
[54] I. Devesa Giner, A. Genazzani, T. Pirali, A. Fernandez Carvajal, A.V. Ferrer Montiel, TRPV1 Modulator Compounds, 2018. WO2018206742.
[55] R.B. Kargbo, TRPV1 modulators for the treatment of pain and inflammation, ACS Med. Chem. Lett. 10 (2) (2019) 143–144, https://doi.org/10.1021/acsmedchemlett.8b00618.
[56] L. Banfi, A. Basso, C. Lambruschini, L. Moni, R. Riva, The 100 facets of the Passerini reaction, Chem. Sci. 12 (47) (2021) 15445–15472, https://doi.org/10.1039/D1SC03810A.
[57] G. Appendino, N. Daddario, A. Minassi, A.S. Moriello, L. De Petrocellis, V. Di Marzo, The taming of capsaicin. Reversal of the vanilloid activity of *N*-acylvanillamines by aromatic iodination, J. Med. Chem. 48 (14) (2005) 4663–4669, https://doi.org/10.1021/jm050139q.
[58] N. Bodor, P. Buchwald, Soft drug design: general principles and recent applications, Med. Res. Rev. 20 (1) (2000) 58–101, https://doi.org/10.1002/(SICI)1098-1128(200001)20:1<58::AID-MED3>3.0.CO;2-X.
[59] F. Brunelli, C. Ceresa, L. Fracchia, G.C. Tron, S. Aprile, Expanding the chemical space of drug-like Passerini compounds: can α-acyloxy carboxamides be considered hard drugs? ACS Med. Chem. Lett. 13 (12) (2022) 1898–1904, https://doi.org/10.1021/acsmedchemlett.2c00420.
[60] M. Mroczkiewicz, R. Ostaszewski, A new and general method for the synthesis of tripeptide aldehydes based on the multi-component Ugi reaction, Tetrahedron 65 (20) (2009) 4025–4034, https://doi.org/10.1016/j.tet.2009.03.018.
[61] M. Serafini, A. Griglio, E. Oberto, T. Pirali, G.C. Tron, The use of 2-hydroxymethyl benzoic acid as an effective water surrogate in the Passerini reaction: a straightforward access to α-hydroxyamides, Tetrahedron Lett. 58 (51) (2017) 4786–4789, https://doi.org/10.1016/j.tetlet.2017.11.021.
[62] K.D. Nadezhdin, A. Neuberger, Y.A. Nikolaev, L.A. Murphy, E.O. Gracheva, S. N. Bagriantsev, A.I. Sobolevsky, Extracellular cap domain is an essential component of the TRPV1 gating mechanism, Nat. Commun. 12 (1) (2021) 2154, https://doi.org/10.1038/s41467-021-22507-3.
[63] T. Hua, X. Li, L. Wu, C. Iliopoulos-Tsoutsouvas, Y. Wang, M. Wu, L. Shen, C. A. Brust, S.P. Nikas, F. Song, X. Song, S. Yuan, Q. Sun, Y. Wu, S. Jiang, T.W. Grim, O. Benchama, E.L. Stahl, N. Zvonok, S. Zhao, L.M. Bohn, A. Makriyannis, Z.J. Liu, Activation and signaling mechanism revealed by cannabinoid receptor-G(i) complex structures, Cell 180 (4) (2020) 655–665.e18, https://doi.org/10.1016/j.cell.2020.01.008.
[64] T. Luk, W. Jin, A. Zvonok, D. Lu, X.-Z. Lin, C. Chavkin, A. Makriyannis, K. Mackie, Identification of a potent and highly efficacious, yet slowly desensitizing CB1 cannabinoid receptor agonist, Br. J. Pharmacol. 142 (3) (2004) 495–500, https://doi.org/10.1038/sj.bjp.0705792.
[65] R. de la Torre-Martínez, M.A. Bonache, P.J. Llabrés-Campaner, B. Balsera, A. Fernández-Carvajal, G. Fernández-Ballester, A. Ferrer-Montiel, M.J. Pérez de Vega, R. González-Muñiz, Synthesis, high-throughput screening and pharmacological characterization of β–lactam derivatives as TRPM8 antagonists, Sci. Rep. 7 (1) (2017) 10766, https://doi.org/10.1038/s41598-017-10913-x.
[66] G.M. Morris, R. Huey, W. Lindstrom, M.F. Sanner, R.K. Belew, D.S. Goodsell, A. J. Olson, AutoDock4 and AutoDockTools4: automated docking with selective receptor flexibility, J. Comput. Chem. 30 (16) (2009) 2785–2791, https://doi.org/10.1002/jcc.21256.
[67] E. Krieger, G. Vriend, YASARA View - molecular graphics for all devices - from smartphones to workstations, Bioinformatics 30 (20) (2014) 2981–2982, https://doi.org/10.1093/bioinformatics/btu426.
[68] K. Ozvoldik, T. Stockner, B. Rammner, E. Krieger, Assembly of biomolecular gigastructures and visualization with the Vulkan graphics API, J. Chem. Inf. Model. 61 (10) (2021) 5293–5303.
[69] Y. Duan, C. Wu, S. Chowdhury, M.C. Lee, G. Xiong, W. Zhang, R. Yang, P. Cieplak, R. Luo, T. Lee, J. Caldwell, J. Wang, P. Kollman, A point-charge force field for molecular mechanics simulations of proteins based on condensed-phase quantum mechanical calculations, J. Comput. Chem. 24 (16) (2003) 1999–2012, https://doi.org/10.1002/jcc.10349.
[70] M.F. Adasme, K.L. Linnemann, S.N. Bolz, F. Kaiser, S. Salentin, V.J. Haupt, M. Schroeder, Plip 2021: expanding the scope of the protein–ligand interaction profiler to DNA and RNA, Nucleic Acids Res. 49 (W1) (2021) W530–W534, https://doi.org/10.1093/nar/gkab294.